Deposition of TiO$_2$-Coated CsPbBr$_3$ Perovskite Heterostructure Thin Film

Miss Chutikan Sairot

A Thesis Submitted in Partial Fulfillment of the Requirements

for the Degree of Master of Engineering in Chemical Engineering

Department of Chemical Engineering

FACULTY OF ENGINEERING

Chulalongkorn University

Academic Year 2020

การปลูกฟิล์มบางโครงสร้างวิวิธพันธุ์ของ $CsPbBr_3$ ที่เคลือบด้วย TiO_2

น.ส.ชุติกาญจน์ สายโรจน์

Thesis Title	Deposition of TiO$_2$-Coated CsPbBr$_3$ Perovskite Heterostructure Thin Film
By	Miss Chutikan Sairot
Field of Study	Chemical Engineering
Thesis Advisor	Assistant Professor Paravee Vas-Umnuay, Ph.D.
Thesis Co Advisor	Professor Tetsuya Kida, Ph.D.

Accepted by the FACULTY OF ENGINEERING, Chulalongkorn University in Partial Fulfillment of the Requirement for the Master of Engineering

-- Dean of the FACULTY OF ENGINEERING

(Associate Professor SUPOT TEACHAVORASINSKUN, Ph.D.)

THESIS COMMITTEE

-- Chairman

(CHALIDA KLAYSOM, Ph.D.)

-- Thesis Advisor

(Assistant Professor Paravee Vas-Umnuay, Ph.D.)

-- Thesis Co-Advisor

(Professor Tetsuya Kida, Ph.D.)

-- Examiner

(Rungthiwa Methaapanon, Ph.D.)

-- External Examiner

(Assistant Professor Weekit Sirisaksoontorn, Ph.D.)

ชุติกาญจน์ สายโรจน์ : การปลูกฟิล์มบางโครงสร้างวิวิธพันธุ์ของ CsPbBr$_3$ ที่เคลือบ
ด้วย TiO$_2$. (Deposition of TiO$_2$-Coated CsPbBr$_3$ Perovskite Heterostructure
Thin Film) อ.ที่ปรึกษาหลัก : ผศ. ดร.ปารวี วาศน์อำนวย, อ.ที่ปรึกษาร่วม : ศ. ดร.เทสุ
ย่า คิดา

การศึกษาการสังเคราะห์สารประกอบ CsPbBr$_3$ เพอรอฟสไกต์ควอนตัทดอทเคลือบ
ด้วยไทเทเนียมไดออกไซต์เพื่อพัฒนาความเสถียรต่อปัจจัยต่าง ๆ ในสภาพแวดล้อม เช่น
ผลกระทบจากน้ำและออกซิเจนในอากาศ เป็นต้น ทำได้โดยการฉีดไทเทเนียมเตตระไอโซโพรพ
อกไซต์ลงไประหว่างการเกิดผลึกของ CsPbBr$_3$ ควอนตัทดอท สารประกอบ CsPbBr$_3$ เพอรอฟส
ไกต์ควอนตัทดอทเคลือบด้วยไทเทเนียมไดออกไซต์ที่สังเคราะห์ได้ มีขนาดผลึก ประมาณ 13 นา
โนเมตร ซึ่งเพิ่มจากควอนตัมดอทที่ไม่ได้ถูกเคลือบมา ประมาณ 1 นาโนเมตร และไทเทเนียมได
ออกไซต์เกิดในลักษณะเฟสอสัณฐาน สารประกอบ CsPbBr$_3$ เพอรอฟสไกต์ควอนตัทดอท
เคลือบด้วยอสัณฐานเฟสของไทเทเนียมไดออกไซต์ ช่วยเพิ่มคุณสมบัติการดูดซับแสงในช่วงแสง
ที่ตามองเห็น นอกจากนี้ ยังช่วยเพิ่มคุณสมบัติในการเคลื่อนที่ของอิเล็กตรอนออกมาจาก
CsPbBr$_3$ ควอนตัมดอท ซึ่งทั้งสองคุณสมบัตินี้ส่งผลดีต่อการเพิ่มประสิทธิภาพของเซล
แสงอาทิตย์ จากการศึกษากระบวนการกำจัดลิแกนด์โดยการเหวี่ยงด้วยสารละลายเมทิลอซิ
เตท พบว่า การเพิ่มจำนวนครั้งในการล้าง จนถึงสามครั้ง สามารถกำจัดลิแกนด์ที่ล้อมรอบ
ควอนตัมดอทได้เพิ่มขึ้น แต่ยิ่งทำให้ขนาดอนุภาคควอนตัมดอทใหญ่ขึ้น ซึ่งส่งผลให้เกิด
ข้อบกพร่องกับฟิล์มบางควอนตัมดอทมากขึ้น การล้างสองครั้งจึงเป็นจำนวนครั้งที่เหมาะสมเพื่อ
กำจัดลิแกนด์ เนื่องจาก สามารถกำจัดลิแกนด์ได้ส่วนหนึ่ง และไม่ทำให้เกิดข้อบกพร่องกับฟิล์ม
บางควอนตัมดอทมากนัก จากนั้น CsPbBr$_3$ เพอรอฟสไกต์ควอนตัทดอทเคลือบด้วยอสัณฐาน
เฟสของไทเทเนียมไดออกไซต์ถูกนำไปขึ้นรูปเป็นชั้นดูดซับแสงสำหรับเซลล์แสงอาทิตย์ และ
สามารถวัดประสิทธิภาพได้ 0.00032% ซึ่งมากกว่าวัสดุที่ไม่ได้เคลือบด้วยไทเทเนียมไดออกไซต์
ถึง 6 เท่า

สาขาวิชา	วิศวกรรมเคมี	ลายมือชื่อนิสิต
		....
ปี	2563	ลายมือชื่อ อ.ที่ปรึกษาหลัก
การศึกษา		....
		ลายมือชื่อ อ.ที่ปรึกษาร่วม
		....

6170147921 : MAJOR CHEMICAL ENGINEERING

KEYWORD: All-inorganic perovskite quantum dots/ TiO2 surface coating/ CsPbBr3/TiO2 quantum dot solar cell

Chutikan Sairot : Deposition of TiO_2-Coated $CsPbBr_3$ Perovskite Heterostructure Thin Film. Advisor: Asst. Prof. Paravee Vas-Umnuay, Ph.D. Co-advisor: Prof. Tetsuya Kida, Ph.D.

All-inorganic lead halide perovskite quantum dots have been emerged in recent years for optoelectronic and photovoltaic devices due to their excellent optical properties. In this work, surface coating was carried out by titanium dioxide (TiO_2) to coat on the surface of $CsPbBr_3$ PQDs to improve the stability and charge separation property. The FTIR spectra confirmed the formation of TiO_2 with an amorphous phase (am-TiO_2). The crystallite size of $CsPbBr_3$/am-TiO_2 QDs composite was increased to be 13.30 nm from 12.65 nm of $CsPbBr_3$. A slightly decrease of energy bandgap was found compare to $CsPbBr_3$ QDs owing to quantum confinement effect. The results also show the enhancement of light absorption in the visible region and charge separation property examined by UV-visible and PL spectroscopy, respectively. The ligand removal process was also investigated by centrifugation of the colloidal QDs with methyl acetate. 2 times washing cycles is the optimal number of times to remove surface ligand due to large amount of ligands were removed and shows less defect in QDs thin film. Finally, $CsPbBr_3$/am-TiO_2 QDs composite was deposited as an absorber layer for the Schottky solar cell device by spin coating technique. The $CsPbBr_3$/am-TiO_2 QDs composite-based solar cell device shows large fill factor up to 86.43% and the best power conversion efficiency (PCE) is 0.00032%, which is about 6 times higher than that of bare $CsPbBr_3$ QDs device.

Field of Study:	Chemical Engineering	Student's Signature
		....
Academic Year:	2020	Advisor's Signature
		....
		Co-advisor's Signature

ACKNOWLEDGEMENTS

TABLE OF CONTENTS

TABLE OF FIGURES

CHAPTER I

INTRODUCTION

1.1 Introduction

Fossil fuels for example coal and natural gas are the main energy sources to produce electricity in the world. However, they are non-renewable and unsustainable which can cause the emission of greenhouse gases and other environmental damages. [1] In order to limit and reduce the environmental degradation, replacing these unsustainable energy sources with renewable energies from renewable natural resources (such as sunlight, wind, rain, tides, waves, and geothermal heat) is necessary. Solar energy is considered to be one of the promising alternatives of renewable and sustainable energy used to provide electricity, because it is very abundant, clean, free and inexhaustible. [2]

Solar cell or photovoltaic cell is an electrical device used for converting solar energy from the sun light directly into the electrical current. Technology of solar cells can be categorized into three generations; the first generation of solar cells are made from crystalline silicon material. This generation is the most popular solar cell technology which show the highest efficiencies compared to other subsequent technologies. Nevertheless, there have been some limitations with the high manufacturing cost due to the cost of silicon, complex and expensive fabrication processes. The second generation of solar cells are known as thin-film solar cells. These solar cells are made from semiconductor materials such as amorphous silicon, cadmium telluride (CdTe), copper indium selenide (CIS) and copper indium gallium (CIGS). This generation shows lower cost of material and manufacturing compared to silicon solar cells, but some of the materials are harmful to the environment and the efficiencies are lower. Due to the high cost of the first generation

and the toxicity of the second generation of solar cells, the third generation of solar cells are now under extensive research and development to produce low cost of manufacturing and high efficiency solar cells. This generation are solution processable solar cells with an excellent potential for large-scale solar electricity generation. [3] The third generation of solar cells include organic solar cells, dye-sensitized solar cells (DSSCs), quantum dot solar cells (QDSCs), and perovskite solar cell (PSCs). PSCs have a rapid rise in the power conversion up to over 25.2% in 2019 from 3.8% of the first report [4] within ten years, as shown in figure 1.1. With the potential of high efficiency, low cost of material and simple method manufacturing [5], this type of solar cell has become one of the great candidates for commercial solar cells.

Perovskite is a material that has the same crystal structure as calcium titanium oxide ($CaTiO_3$) with a general chemical formula of ABX_3, where A can be replaced with an organic component such as methylammonium (MA^+) or formamidinium (FA^+) or an inorganic atom such as cesium (Cs^+), B is a transition-metal cation for instant Pb^{2+} and Sn^{2+}, and X is a halide anion such as Cl^-, Br^-,and I^-). Perovskite materials have been applied to various optoelectronic and photovoltaic applications such as light emitting diodes, lasers, solar cells and more, due to their intrinsic optoelectronic properties such as broad absorption spectrum, fast charge separation, long transport distance of electrons and holes and long carrier separation lifetime.

An organic-inorganic hybrid perovskite material (such as methylammonium lead iodide ($MAPbI_3$) and formamidinium lead iodide ($FAPbI_3$)) is the most commonly used as an active layer in the perovskite solar cell. However, perovskite containing volatile organic component such as MA^+ and FA^+ shows less stability in ambient conditions from the occurrence of hydration reaction, leading to the decomposition of crystal structure. [6] Therefore, all-inorganic perovskite $CsPbX_3$ (X = Cl, Br, I or mixed halides) with higher chemical and thermal stability, compared to the hybrid organic-inorganic perovskite, has

been attracting significant interest in recent years. In particular, $CsPbBr_3$ has shown the most superior stability among other inorganic perovskites. Unfortunately, the deposition of $CsPbBr_3$ thin film with high compact, smoothness, less pinholes, and large grain size for high performance photovoltaic device is difficult due to the crystallization process during the film deposition. These problems could be attributed to many factors including precursor ratio, evaporation of solvent, process additive, annealing temperature etc. Therefore, size reduction of particles into nanoparticle or quantum dot (QD) scale can be one of the solutions to eliminate crystallization process and decouple grain growth from film deposition. [7]
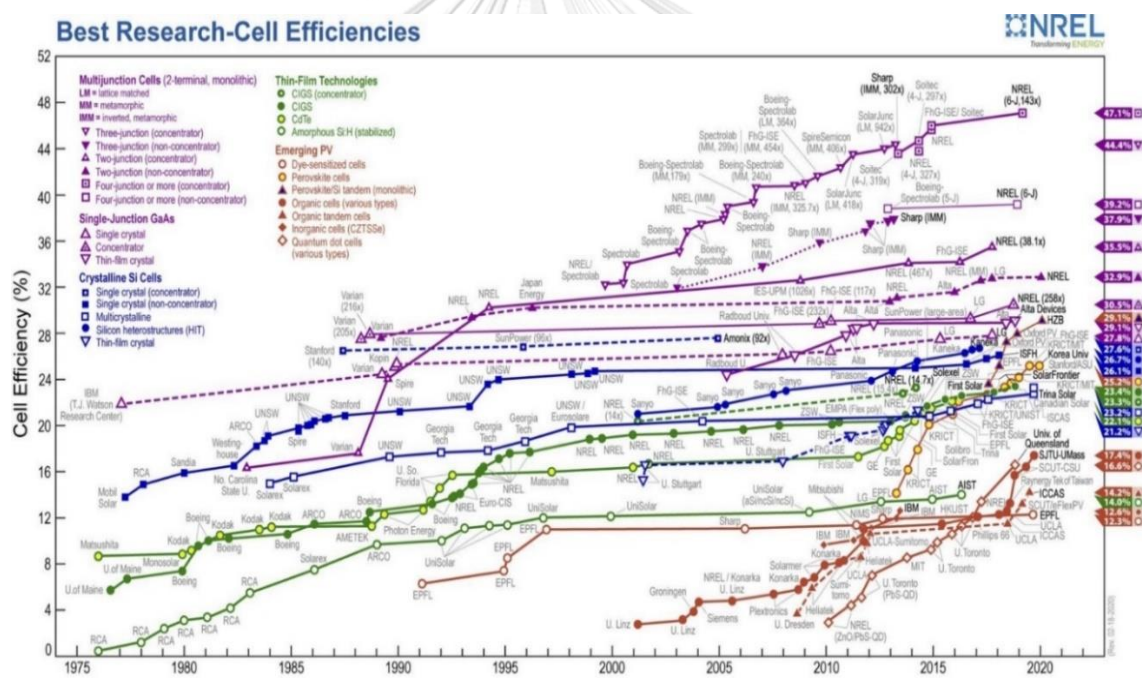
Figure 1. 1 The development conversion efficiencies for research cells. [8]

Recently, perovskite quantum dot solar cells (PQDSCs) have emerged as one of the promising candidates for high-performance photovoltaic and other optoelectronic devices due to their bandgap tunability, high photon absorption coefficient and facile solution processability. [9] In the past decade, the power conversion efficiency of

PQDSCs has increased up to 16.6% in 2019, as shown in **figure 1.1**. Different types of solar cell device architectures also play important roles in quantum dots solar cells (QDSCs). There are three types of QDSCs architecture have been developed, including 1) a Schottky junction, 2) depleted QD-based heterojunction cell, and 3) quantum dot sensitized solar cells, the device structure was shown in **figure 1.2**. [10] In among of device structure, Schottky junction solar cells have the merits of simple device fabrication process, low cost of manufacturing, and commercially available, it can be formed by depositing a semiconducting QD layer directly on transparent metal oxide (FTO or ITO) to form Ohmic contact, while depositing a metal (e.g., Al, Ag, Au) on QD layer to form a Schottky junction. [11]
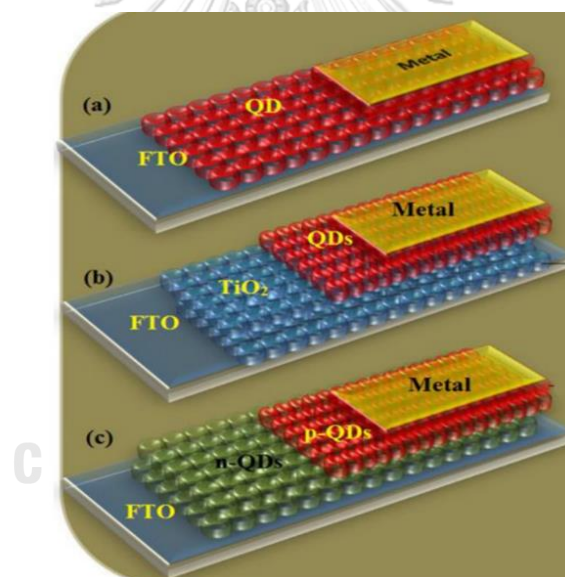
Figure 1. 2 QDSC device: (a) QD Schottky junction cells,

(b) Depleted QD heterojunction cells, (c) Quantum junction solar cells. [10]

Nevertheless, the main issue of PQDs suppressing broad applications is their poor stability in moisture and oxygen due to the strong water and oxygen absorption behavior of halide elements, leading to aggregation of QD particle, structure degradation and decreasing in QD performance. [12]

In order to improve the stability of PQDs, surface coating with inorganic materials (such as silica, AlO_x and polymer) has been studied to form a water-proof matrix protecting QDs from moisture and oxygen in the air. [12] Even though formation of inorganic shell passivated at surface of QDs can prevent moisture and oxygen degradation, it cannot maintain a charge transport property of these QDs, resulting in decreasing device performance when applied in optoelectronic and photovoltaic applications. Zhi-Jun Li and co-workers synthesized titanium dioxide (TiO_2) shell-coated $CsPbBr_3$ nanocrystals (NCs) by encapsulation of colloidal $CsPbBr_3$ NCs with titanium precursor.

$CsPbBr_3/TiO_2$ showed a long-term stability over 80 days in the presence of water and it could maintain charge transport property due to conductivity of the TiO_2 shell. [13] Due to the merits of chemical and thermal stability and good conductivity of TiO_2, it could enhance the charge separation and charge transport properties of $CsPbBr_3$ perovskite. This is possible that coating with TiO_2 not only improves the stability of QD but also maintains a charge transport property of perovskite material and increases electron extraction rate from the perovskite material leading to the reduction of the electron and hole recombination in solar cell device, which is crucial for a good solar cell performance. This approach can offer a new way to improve power conversion efficiency (PCE) of the perovskite solar cell.

Herein, we developed a new simple strategy for coating TiO_2 on the surface of $CsPbBr_3$ PQDs by hot-injection and investigated the effects of TiO_2 coating on the optical properties of $CsPbBr_3$ QD. The enhancement of charge transport property of the obtained TiO_2-coated $CsPbBr_3$ QD composite could be examined by applying the sample in a solar cell application. In addition, PQDs are typically capped by long chain alkyl ligands such as oleic acid (OA) and oleylamine (OAm). These impurities can form as electrical insulators that inhibit film formation and reduce charge injection from hole and electron

transporting layer and charge transport property in QD film. [14] Therefore, ligand removal process is an important step for thin film deposition. However, QDs are very sensitive to a polar solvent that can cause an optical quenching from decomposition of perovskite QDs structure. Chiba et al. reported that an ester solvent (such as butyl acetate, butanol) can be used as a washing solvent without quenching of QDs. [15] E. Moyen et al. demonstrated the method to remove surface ligand before thin-film deposition by adding methyl acetate to QDs as a suspended solution to remove weakly bonded long chain ligands from perovskite QDs [16] and X Ling et al. also demonstrated a ligand removal process layer by layer during thin film deposition using methyl acetate as a washing solvent. The PCE of the device was achieved up to 14.1%. [17] In this work, suitable ligand removal processes to produce high film uniformity and solar cell performance of TiO_2-coated $CsPbBr_3$ QD composite were studied by investigating the effects of ligand removal process on the optical properties and thin-film formation using methyl acetate as a removal solvent.

1.2 Objectives of research

1.2.1 To synthesize TiO_2-coated $CsPbBr_3$ quantum dot composite and investigate the effects of TiO_2 coating on optical properties and charge transport property of $CsPbBr_3$ quantum dots.

1.2.2 To find the optimal condition for the ligand removal process by investigating the effects of washing cycles on optical properties and film morphology.

1.2.3 To investigate the effects and compare between bare $CsPbBr_3$ and $CsPbBr_3$ coated TiO_2 quantum dot composite, used as an absorber layer in perovskite solar cells in terms of solar cell performance.

1.3   Scopes of research

The study of this research was divided into three parts. The first part is the synthesis of TiO_2-coated $CsPbBr_3$ QD composite. The second part is the study of ligand removal process to find the optimal condition for removing surface ligand by investigating the effects of washing cycles of TiO_2-coated $CsPbBr_3$ QD composite on optical properties and film morphology, which is crucial for a solar cell performance. The third part is the deposition of the obtained TiO_2-coated $CsPbBr_3$ QD composite used as an absorber layer in solar cell device by spin coating technique to investigate and compare the effect of bare $CsPbBr_3$ and TiO_2-coated $CsPbBr_3$ QD composite on solar cell performance. The followings describe the experimental and characterization method of each part.

1.3.1   Synthesis of TiO_2 coated $CsPbBr_3$ ($CsPbBr_3/TiO_2$) QD composite

The $CsPbBr_3/TiO_2$ QD composites were synthesized via hot injection by injection of titanium tetraisopropoxide (TTIP) as a titanium precursor. The obtained $CsPbBr_3/TiO_2$ QD composite were then characterized as follows:

- **X-ray diffraction (XRD):** to examine the crystal structure and phase of TiO_2 formation on $CsPbBr_3$ crystal structure.

- **UV-visible spectroscopy and photoluminescence (PL) measurement:** to measure light absorption spectra and emission spectra

- **Fourier-transform infrared spectroscopy (FTIR):** to confirm phase of titanium and titanium component on $CsPbBr_3/TiO_2$ QD composite

- **Transmission electron microscopy (TEM):** to measure crystallite size and observe the formation of TiO_2 on $CsPbBr_3$

1.3.2 Ligand removal process

This process was carried out by washing the obtained CsPbBr$_3$/TiO$_2$ QD composite with the removal solvent, which is the mixture of toluene and methyl acetate, in order to remove the long chain surface ligands. By the way, the QD composite need to be washed many times to remove all of the surface ligand but larger amount of the ligand loss can affect the optical properties of QD. Therefore, the optimal washing cycle was studied by investigating the effects of number of washing cycles (0 to 3 cycles) on the optical properties and film morphology. The removal of surface ligands was characterized by FTIR. The effects of increasing the number of QD washing cycles on optical properties, including light absorption property and optical bandgap were characterized by UV-visible spectroscopy and Tauc's plot, respectively. The particles size and particles size distribution were examined by dynamic light scattering (DLS) measurement. Finally, the QD films prepared from each sample were observed under UV light irradiation to observe the effect on film morphology.

1.3.3 Perovskite solar cell fabrication

The perovskites solar cell devices were fabricated with the structure as shown in **figure 1.3**. To eliminate the effect from the electron and hole transporting layer the device was prepared as a pattern of Schottky junction solar cell device. The QD active layer, including CsPbBr$_3$ and CsPbBr$_3$/TiO$_2$ QD composite were deposited by spin-coating technique on the FTO coated glass substrate. The gold (Au) electrode deposited by thermal evaporation technique was used as a counter electrode which receives hole and makes a complete electric circuit. The characterization techniques required for the investigation of the film morphology and solar cell performance can be described as follows.

- **Scanning electron microscopy (SEM)**: to observe morphology and thickness of perovskite thin films

- **Current-voltage characteristic measurement**: to measure the I-V characteristic of the perovskite quantum dot solar cell devices and calculate the solar cell performance parameters, including photocurrent density-voltage (J-V) curve, open circuit voltage (V_{oc}), Fill factor (FF), and power conversion efficiency (PCE)
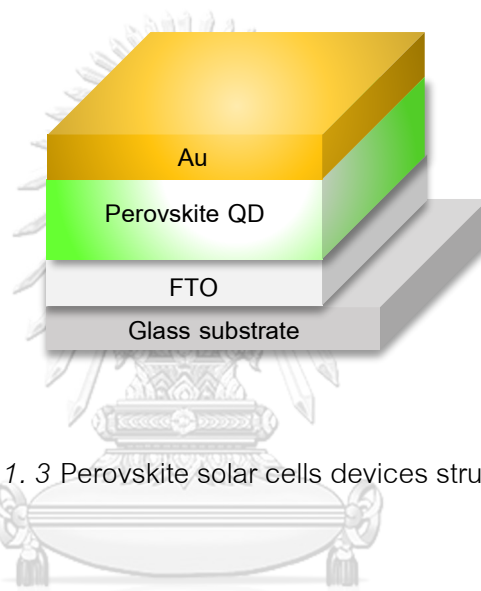
Figure 1. 3 Perovskite solar cells devices structure.

CHAPTER II

THEORY AND LITERATURE REVIEW

2.1   Fundamental of Solar cell

Solar cell or optoelectronic device is the device to harvest solar radiation and convert into electricity. When the sunlight strikes on the solar cell surface, the active material (p-n junction) is excited by absorbed photon with equal or higher energy compared to the energy bandgap (E_g) of the active material. Then the cell generates the electron and hole carriers, followed by the collection of these carriers by the p-n junction. Holes are collected in a positive or p-type semiconductor and electrons are collected in a negative or n-type semiconductor. [18] When a circuit is made, free electrons have to pass through the load to recombine with positive holes. Current can be generated from the cells under illumination. Figure 2.1 shows how the solar cell works. [19]
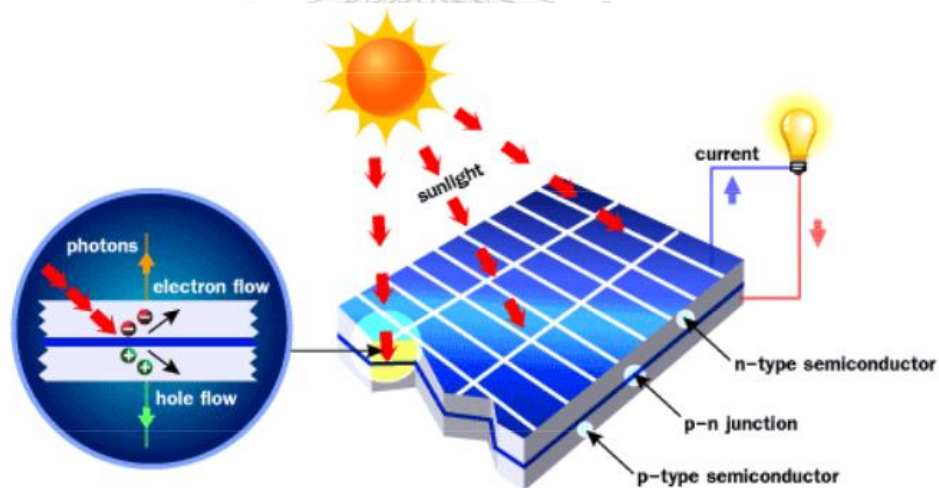
Figure 2. 1 Schematic of solar cell working. [19]

2.1.1   Measure of solar cell performance

The performance of solar cell can be characterized by measurement of the current density by varying the load during device irradiation by light. The power conversion efficiency (PCE) is the most fundamental measurement of solar cell performance. It is defined as the ratio of the electric power delivered to the external circuit to the solar power incident on the cell, as shown in eqn. 1:

$$PCE = \frac{P_{out}}{P_{solar}} = \frac{J_{sc}V_{oc}FF}{P_{solar}}$$

(1)

Where J_{sc} is the short-circuit current density

V_{oc} is the open circuit voltage

FF is the fill factor

P_{solar} is the incident power

The fill factor FF is defined as

$$FF = \frac{J_{max}V_{max}}{J_{sc}V_{oc}}$$

(2)

It is the power produced at the maximum power point on the J-V curve divided by the product of V_{oc} and J_{sc}. It can be thought as a measurement of how rectangular the   J-V characteristic is in the fourth quadrant. [20]

2.1.2 Classification of solar cells

The classification of solar cells is divided into three categories:

2.1.2.1 Crystalline silicon solar cells

This is the 1st-generation of solar cells based on crystalline silicon material (c-Si). This generation is the oldest solar cell technology and the most available used and sold in the market until now because silicon solar cells are the most efficient in terms of single cell photovoltaic devices, and very abundant material on earth. [21] Furthermore, this material is a semiconductor material with an energy bandgap of 1.1 eV which is suitable for photovoltaic applications. This makes silicon still the most popular solar cell until now. Crystalline silicon solar cells can be categorized into four main types depending on their fabrication method including monocrystalline, polycrystalline, amorphous silicon, hybrid panels. However, the conventional silicon solar cells have higher production costs and high cost of electronic grade silicon wafers.

2.1.2.2 Thin-film solar cells

The 2nd-generation of solar cells are based on thin film technology because they can be made in much thinner and lighter formats compared to the 1st -generation solar cell. This generation is made by depositing two heterojunction layers between two contact layers. The chalcopyrite-based compounds such as CdTe or CIGS and amorphous silicon thin film are used as a material in this generation. These materials are cheap when compared to c-Si based solar cells, However, these materials are limited by

exceedingly toxic of cadmium. Furthermore, their efficiency is lower than 1st-generation and they are usually deposited by vacuum-assisted or by chemical vapour deposition (CVD) which is costly for large scale fabrication.

2.1.2.3 Organic solar cells

By contrast to 1st and 2nd generation, the 3rd-generation of solar cells are derived from solution process. This generation is much more advantageous because of the possibilities of tuneable bandgap, ability to harvest light from various parts of the solar spectrum, fabrication of the devices on flexible substrates, and molecule-to-molecule interactions. This generation includes OPVs, perovskite solar cells, dye-sensitised solar cells (DSSCs), and quantum dot solar cells. Classification of solar cells is shown in Figure 2.2.
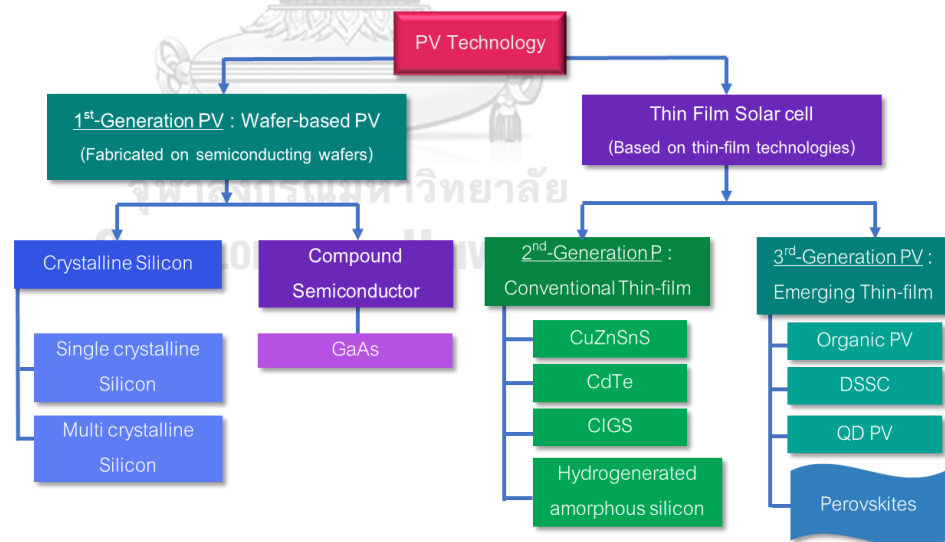
Figure 2. 2 Classification of photovoltaic technologies. [22]

2.2   Perovskite solar cells (PSCs)

2.2.1   The architecture of PSCs

Generally, the PSC architecture is classified into two main different types including mesoporous structure and simple planar heterojunction. Moreover, these two types of PSC structure are divided into conventional n-i-p and invert p-i-n architecture, in accordance with the location of ETL and HTL in the device layer stack. The mesoporous PSCs are generally composed of glass / compact ETL / mesoporous layer / perovskite / HTL / metal electrode, whereas the planar heterojunction PSCs do not have a mesoporous layer. Thus, the active layer contacts directly with the compact layer, as shown in figure 2.4.
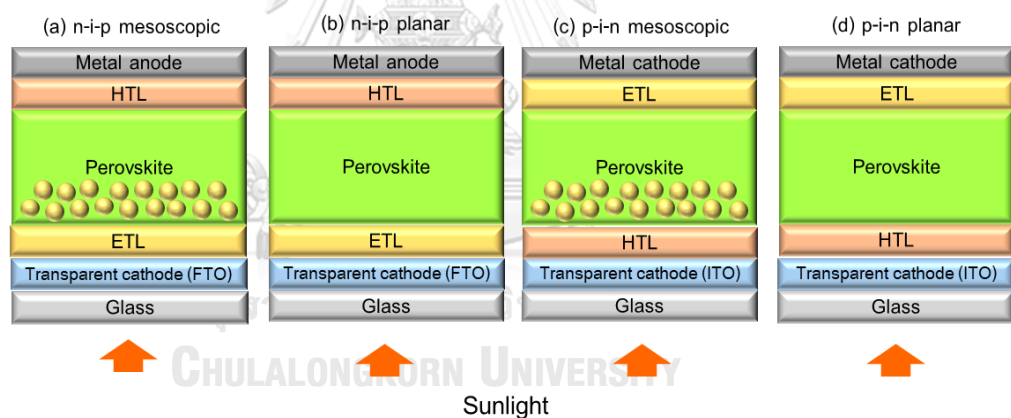
Figure 2. 3 Schematic diagrams of perovskite solar cells in the: (a) n-i-p mesoscopic, (b) n-i-p planar, (c) p-i-n mesoscopic structures, and (d) p-i-n planar; (a,b) Normal device structure; and (c,d) inverted device structure.

2.2.2 Light absorption and generation of free carriers in PSCs

Figure 2.4 shows working mechanism of PSCs involving the following steps: first, photon absorption of perovskite material, second, free charge carriers (electrons and holes) generation, third, charge transport by separation of electron and hole, the photogenerated electron transfers into the ETL and migrates to the anode. Then, passes through the external circuit to the cathode. At the same time, the hole transfers into the HTL, then migrates to the cathode and makes a complete electrical circuit. In this process, conduction band of ETL should have a lower energy level than perovskite active layer to allow electron transfer from perovskite material. Similarly, HTL should have a lower valence band energy level than valence band energy of perovskite material for hole transporting.
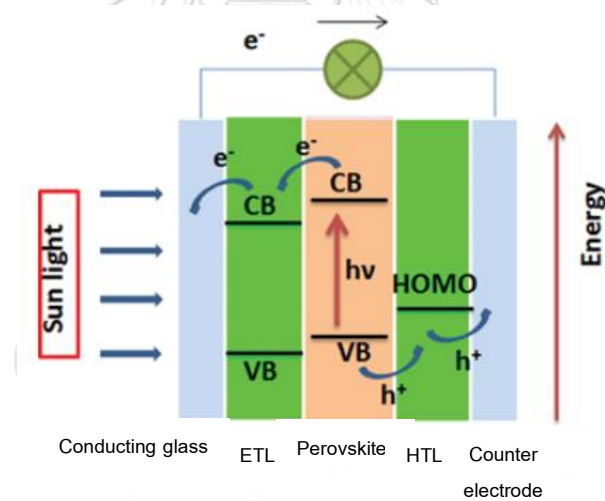
Figure 2. 4 Band diagram and main processes of PSCs. 1. Absorption of photon and free charges generation; 2. Charge transport; 3. Charge extraction [23]

2.3   Quantum Dots Solar cells (QDSCs)

Recently, organic-inorganic lead halide perovskite and inorganic perovskite quantum dot solar cell have provided a new alternative for the third generation of solar cells due to the advantages of low-cost materials, a cost-effective solution processing, and commercially available. QDs have the advantage of tunable bandgap by tuning their size or chemical composition. The adjustable bandgap of quantum dots allows the construction of nanostructured solar cell that is able to harvest more of the solar spectrum. QDSC architectures can be classified into four types, as shown in figure 2.5 [10] :

1) QD Schottky junction cells

2) Depleted QD heterojunction cells

3) Quantum junction solar cells

4) QD sensitized solar cells
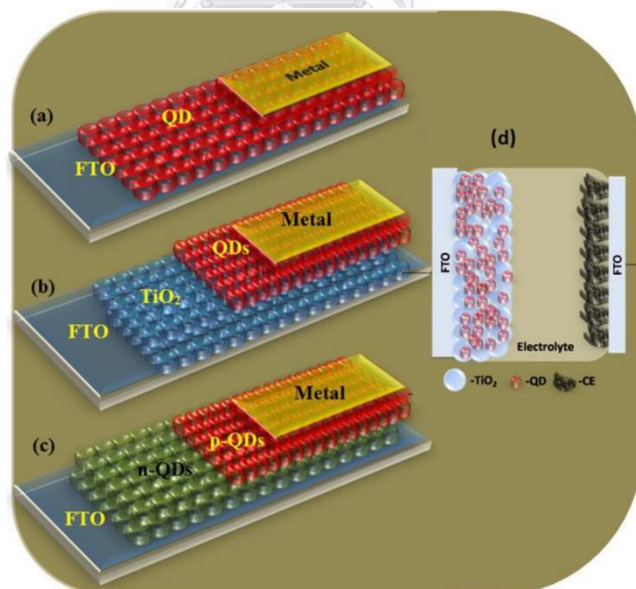
Figure 2. 5 QDSC device: (a) QD Schottky junction cells, (b) Depleted QD heterojunction cells, (c) Quantum junction solar cells, (d) QD sensitized solar cells [10]

In this work, we will focus on the QD Schottky junction cells or metal-semiconductor junction solar cell. It is basically fabricated from quantum dots layers (Nanocrystals film) sandwiched between metallic electrode and ITO counter electrode deposited on transparent glass substrate to act as photo-electrode. In the band diagram shown in Figure 2.6 depletion region is due to charge transfer to QD film. Because of high electron density in metal (~ 1022 cm^{-3}), the depletion is negligible on its side of the cell.
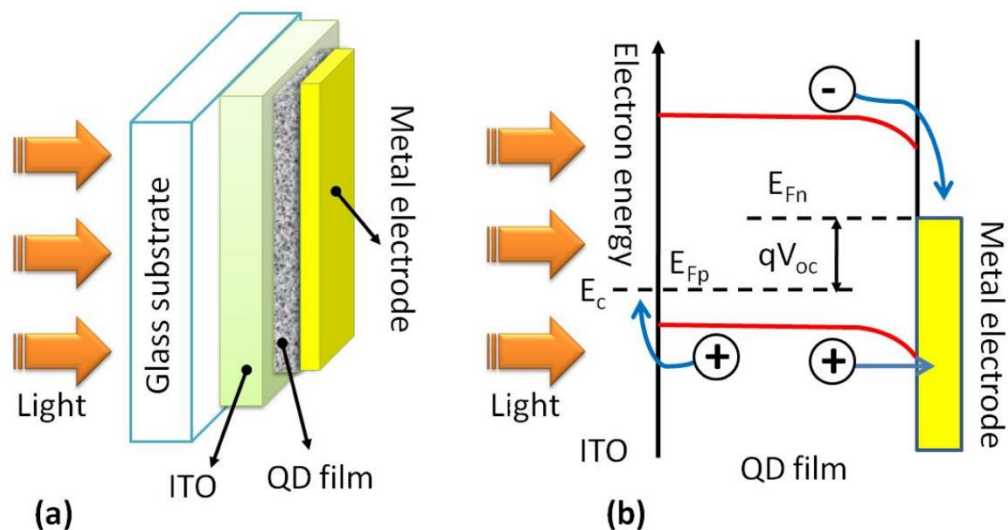
Figure 2. 6 (a) Schematic of Schottky barrier quantum dots based solar cell, (b) band diagram of Schottky solar cell. [10]

2.4   What are perovskites?

Perovskites is a name of $CaTiO_3$ mineral, with a crystal structure ABX_3. Perovskites appear particularly attractive as next- generation of solar devices because their high-power conversion efficiency (PCE) and solution processability. Perovskites have rapid development since the first report in 2009 by Miyasaka et al. [4] and in the past decade perovskite solar cell can achieve PCE up to over 25.2%. [8]

Organic-inorganic halide perovskites have a chemical formula ABX_3 where A-site is occupied by monovalent cation (e.g., methylammonium (MA^+) $CH_3NH_3^+$, formamidinium (FA^+) $CH_2(NH_2)_2^+$), or inorganic cation (e.g., Cs^+, Rb^+, K^+); B-site by a divalent cation (e.g., Pb^{2+}, Sn^{2+}, Ge^{2+}); X-site by halogen anion (e.g., I^-, Br^-, Cl^-). In an ideal case, the halide perovskite structure is a cubic structure, as shown in figure 2.7. [24] B-site and X-site are coordinate as a BX_6^{4-} octahedra to pack as a cubic structure. The size of cation A located at the center of BX_6^{4-} octahedral should be suitable for the formation of close-packed perovskite structure. [6] Deviation from cubic symmetry can result from several factors such as the first being size effects and tolerance factor, developed by Goldschmidt in 1927, tolerance factor is defined by:

$$\tau = \frac{(R_A + R_x)}{\sqrt{2}(R_B + R_X)} \tag{3}$$

where R_A, R_B and R_X are the ionic radii of the A, B and X site ions, respectively. Generally, the accepted tolerance factor for halide perovskite is lied in the range of $0.85 < \tau < 1.11$. [25]
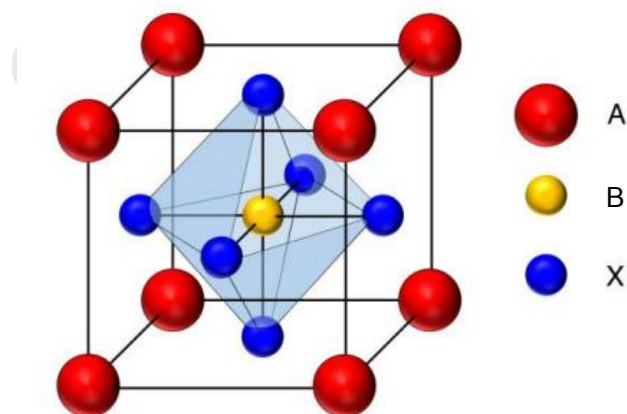
Figure 2. 7 Perovskite generic crystal structure. [24]

2.5   Perovskite quantum dots (PQDs)

Semiconducting quantum dots offer important advantages over conventional bulk materials such as solution-processability, low-temperature fabrication, and quantum size effect tunability of their bandgap, which allows their absorption properties to be optimized for optoelectronic and photovoltaic applications.

2.5.1   What are quantum dots?

Quantum dots (QDs) or nanocrystals (NCs) are a special class of semiconductor material with a diameter in a few nanometers. One of the most observations when reducing the size of materials to the nanometer scale is the confinement in the movement of electrons due to the quantum confinement effect. Depending on a very small size, when the semiconductor absorbs light, leading to an electron being excited from valence band to the conduction band leaving a hole at the valence band, these electrons which are confined in small space (quantum box) can bind to the holes to form exciton. When this exciton recombines, the exciton's energy can be emitted as light called fluorescence. Generally, decreasing of the crystal size results in increasing of energy gap between the highest valence band and the lowest conduction band. Therefore, more energy is then needed to excite the dot, and more energy is released when the crystal returns to its ground state, resulting in a color shift from red to blue in the emitted light. This phenomenon indicates emission color tuneability of nanomaterials by changing size of particles, as shown in **figure 2.8**.
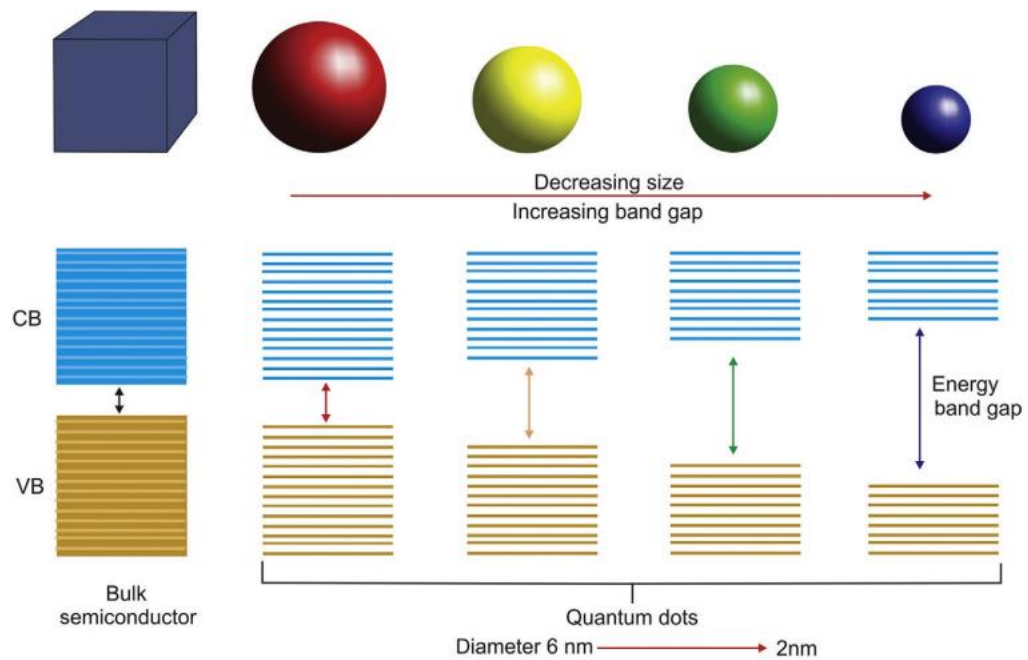
Figure 2. 8 Energy band variation in quantum dots as the size is varied. [26]

QDs can be classified into three types according to dimensionality of nanocrystal. Dimensionality of QDs is defined as the number of directions that the carriers are free to move consist of:

Quantum Well (QW): These are thin film structures (**figure. 2.9**) with a few nanometer thickness. They are also defined as two-dimensional (2D) structures because the particle is free to move in two directions, while restriction of particle motion occurs in the other direction.

Quantum Wire (QWr): These are one-dimensional (1D) structures in which electrons are free to move in one direction, while quantization occurs in the remaining two directions. They appear like tubes and wires with diameters in the nanometer range and lengths of several micrometers.

Quantum Dots (QDs): They are also identified as semiconductor nanocrystals, nanoparticles, clusters, colloidal nanostructures, and zero-dimensional (0D) objects. These are nanosized crystals composed of several tens to a few thousand atoms. Electrons are quantized in all three directions.

| Bulk material | Quantum well | Quantum wire | Quantum dot |
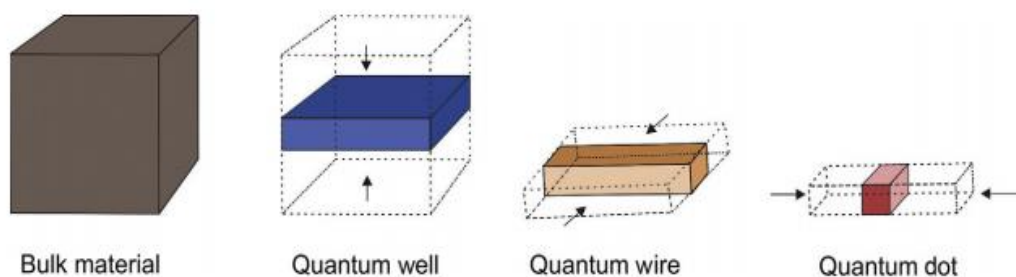
Figure 2. 9 Schematic diagram for quantum nanostructures; bulk material, quantum well, quantum wire and quantum dot. [26]

2.5.2 Optical properties of PQDs

The optical properties of PQDs exhibit remarkable significant for optoelectronic applications with tunable bandgap color and absorption spectra by controlling their chemical composition and crystallite size. Q. le et al. described tuning the bandgap of PQDs by adjusting their composition. Due to compositional flexibility of PQDs, monovalent A-site cation, divalent B-site cation, and X-site halide anion can be mixed or substituted. Therefore, many researchers have attempted to tune the energy bandgap of PQDs by changing and adjusting ratio of halide elements. For example, Protesescu et al. reported tuning energy bandgap of $CsPbX_3$ NCs by adjusting the ratio of halides in mixed halide NCs. The corresponding PL spectra can be tuned from 410 to 700 nm. The NCs show changing in PL emission peak from 410 nm, when X is Cl, to 525 nm, when X is

Br, and to 700 nm, when X is I, as shown in **figure 2.10a-c**. Changing of PL emission spectra indicates changing of energy bandgap in PQDs. [27]

A-site cation substitution with Cs^+, other alkylammonium cations, or a mixture of the two is another possible method for tuning PQDs bandgap. Changing of A-site ionic radius affects the bond length between B-site metal cation and X-site halide anion in the cubic perovskite crystal structure. The correlation between size of the A-site cation and the bandgap energy is observed by comparison the bandgap energy of different A-site cation perovskite materials. For instance, $CsPbI_3$, $MAPbI_3$, and $FAPbI_3$. Due to Cs^+ (1.81 Å) has a smaller ionic radius than MA^+ (2.70 Å) and FA^+ (2.79 Å), Therefore, the bandgap energy of $CsPbI_3$, $MAPbI_3$, and $FAPbI_3$ are 1.73, 1.57, and 1.48 eV, respectively. [28] This indicates the bandgap decreases as the size of the A-site cation increases.

จุฬาลงกรณ์มหาวิทยาลัย
CHULALONGKORN UNIVERSITY
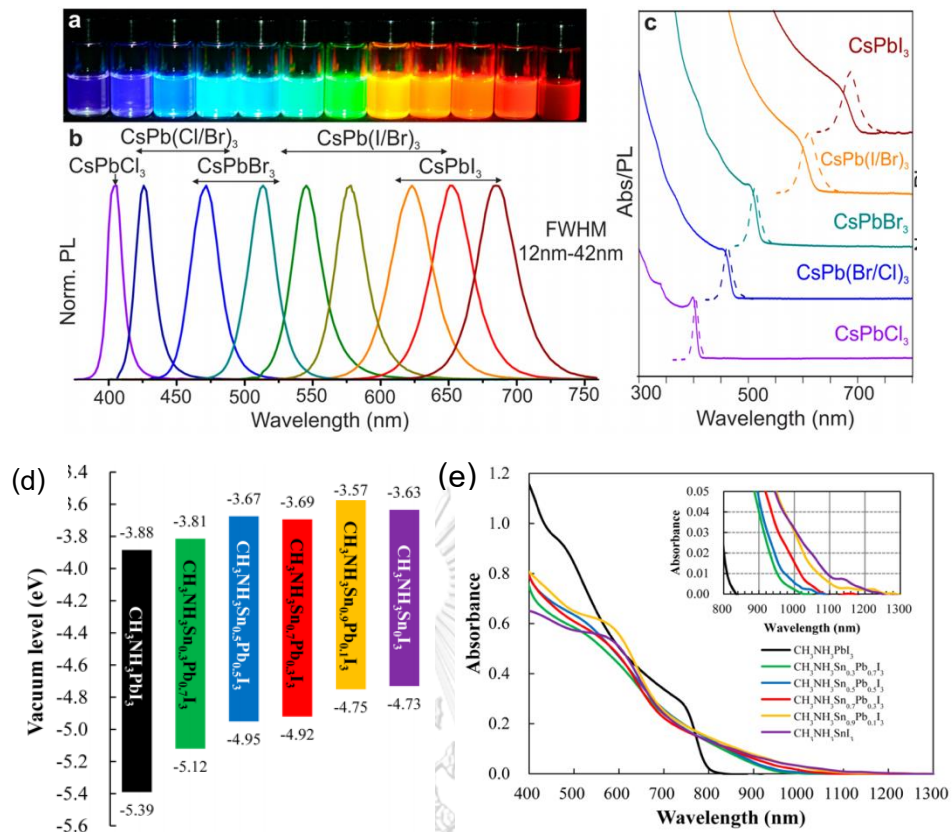
Figure 2. 10 (a) colloidal solutions of perovskite quantum dot under 365 nm UV lamp, (b) representative PL spectra, (c) typical optical absorption and PL spectra. (d) Energy diagram for $CH_3NH_3Sn_xPb_{(1-x)}I_3$ perovskite, (e) $CH_3NH_3Sn_xPb_{(1-x)}I_3$ perovskite coated on porous TiO_2 electronic absorption spectra. [29]

The substitution or mixing of the B-site cations (Pb^{2+}) with other divalent cation such as Cd^{2+}, Mn^{2+}, and Sn^{2+} is another way to tune bandgap of PQDs. Ogomi and co-workers demonstrated mixing of Pb^{2+} with Sn^{2+} in different ratio, the results showed a change in bandgap energy of $CH_3NH_3Sn_xPb_{(1-x)}I_3$ depending on the ratio of Sn to Pb used; The bandgap becomes smaller when x is increased. As shown in **figure 2.10c**, shifting of the valence band was observed for the different Pb/Sn ratio. These results indicate that the bandgap of PQDs can be reduced due to the large valance band shift. According to change in bandgap of

PQDs from inserting the amount of Sn^{2+}, the absorption spectra is also redshifted from 1000 to 1300 nm, as shown in figure 2.10d. [29]

The last significantly factors influence to bandgap tuning of PQDs are dimensionality and size tuning. Dimensionality of a material specifies how many dimensions do the carriers of the material act as free carriers. The low-dimensional nanostructures show significantly different optical properties (bandgap) from bulk perovskite materials due to quantum size effects. As shown in **figure 2.9a**, The density of states (DOS) in bulk materials (3-dimensional materials) is proportional to the square root of energy ($E^{1/2}$), whereas the DOS of 2-dimensional materials exhibits an E^0 dependence for each quantized state, the DOS of 1-dimensional materials shows a $E^{-1/2}$ dependence for single quantized state, and the DOS of zero-dimensional materials is described mathematically by a delta function δ-function.[30]

Many researchers have attempted to tune the band energy of PQD material by controlling their size. L. Protesescu et al. demonstrated effect of changing size to optical properties of $CsPbBr_3$, as shown in figure 2.11b. The $CsPbBr_3$ NCs are blue-shifted when their size is reduced from 12 to 5 nm. [27] The blue-shift of PL emission peak and absorption edge indicate that the bandgap of PQDs can be adjusted by controlling their size.
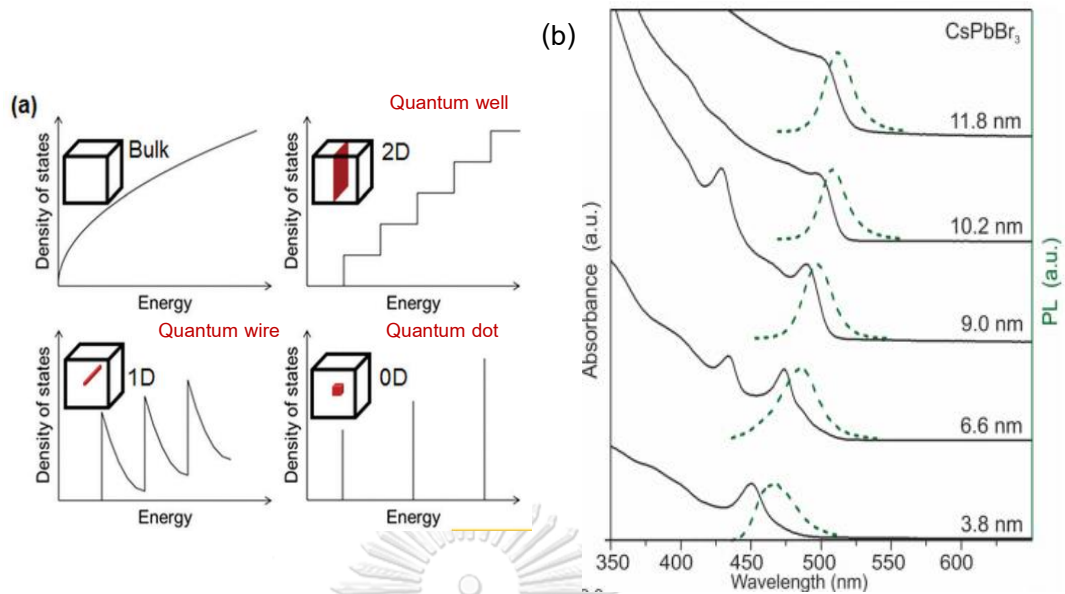
Figure 2. 11 Quantum size effect in nanostructure semiconductors: (a) density of states energy band variation in quantum dots as the size is varied. (b) quantum-size effects in the absorption and emission spectra of 5-12 nm $CsPbBr_3$ NCs.[18]

These excellent optical properties with high color purity emission, color, and bandgap tunability, high photoluminescence, high extinction coefficients and low-cost solution processed colloidal of PQDs make them the most promising candidate for LED application and attractive for the next generation photovoltaics technologies.

2.5.3 Synthesis of PQDs

Generally, organic-inorganic and all-inorganic PQDs were synthesized using solution processes to produce high crystallinity and quantum confinement effects. The methods to prepared PQDs can be divided into two main methods including first, room-temperature solution method consist of ligand-assisted reprecipitation (LARP) and emulsion method, and second is the method which

needs external energy such as heating or high energy wave including hot-injection and top-down synthesis method.

Ligand-assisted reprecipitation technique (LARP): This method is prepared by mixing perovskite precursor (MAX/FAX/CsX and PbX_2) with a good solvent (DMF/DMSO), followed by quickly injecting into a fixed amount of three long-chain coordinate ligand including oleic acid, oleylamine, and n-octylamine mixed with a poor solvent (toluene, hexane, etc.) under a vigorously stirring. The colloidal solution is immediately turned to a yellow-green solution, indicating formation of perovskite nanocrystals. This process is operated at room temperature. [31]

Emulsion method: H. Huang et al. demonstrated synthesis of $MAPbBr_3$ and $CsPbBr_3$ PQDs by emulsion method. An emulsion synthesis method includes two step, emulsion formation and demulsion. Two solutions (A and B) were prepared, solution A is a precursor solution which is a mixing of MAX or CsX and DMF or DI water, respectively, solution B is a mixing of PbX_2 and DMF. Solution A and B were added dropwise into the mixture of n-hexane, oleic acid (OA) and n-octylamine under stirring. The color of solution was immediately changed to yellow after addition of solution B. The mixture was stirred for 5 min and a fixed amount of acetone was added as a demulsifier and stirred for 10 min. The colloidal PQDs were formed. [32] DMF (act as aqueous phase) is insoluble in n-hexane (act as oil phase) formed the emulsion suspension in n-hexane, after addition of acetone (as a demulsifier) the mixture can be turned to single phase and PQDs were formed.

Hot-injection method: The most popular method for synthesis of traditional NCs. Protesescu et al. reported the synthesis of all-inorganic PQDs for the first time using hot-injection method. [27] Cesium oleate was firstly prepared by mixing of cesium carbonate (Cs_2CO_3), octadecene and oleic acid and then the mixture was dried for 1 h at 120 °C and heated under N_2 to 150 °C until all Cs_2CO_3 completely reacted with oleic acid. The Cs precursor solution was then injected into PbX_2 solution (mixture of PbX_2 where X is I, Cl or Br, oleylamine and oleic acid) under a certain temperature and inert gas protection, after injection the solution was immediately cool in ice-water bath. The size of NCs can be affected from reaction temperature. This method also has been applied to synthesis of organic-inorganic PQDs by modifying the related experimental step.

Top-down method: This method shows advantages in polar-solvent-free, single-step strategy, which has been widely used for fabrication of nanocrystal material. In this method, bulk materials will be cut into smaller fragments by external fore until they finally reach nanometer size. An example for this method is an ultrasonication technique, starts by mixing of coordinate ligand or long chain organic surface ligand, cesium carbonate and lead halide precursor under ultrasonication to quickly form bulk perovskite. Then, the bulk perovskite was broken into NCs or QDs under continuous ultrasonication.

In conclusion, LARP and emulsion method show advantages of facile synthesis temperature and procedure and short reaction time. However, PQDs synthesized by these methods have disadvantages with low crystallinity and stability. In contrast, the PQDs synthesized by hot-injection method shows high crystallinity due to high-temperature growth as well as uniform particle sizes. This method is the most popular in the synthesis of PQDs, even if the synthesis steps

of this method are complex. The top-down or ultrasonication method shows long reaction time and various QD particle sizes were achieved.

2.5.4 Stability of PQDs

Due to the instability of PQDs when exposed to ambient conditions, leading to a decomposition of QD structure, particle aggregation and surface ligand detachment. To solve these problems, outer shell coating serves as the most efficient method. There are many methods have been used for coating PQDs, for instance:

Mesoporous Silica: Silica coating is widely used to improve stability in NC materials because silica shell is a transparent material that does not affect optical properties of luminescent material but dramatically improves stability.

Polymer Coating: Raja et al. mixed $CsPbBr_3$ PQDs and polymers in toluene and compared stability and water/oxygen diffusion between three polymers, (PS, poly(styrene-ethylene-butylene-styrene) (SEBS), and poly(lauryl methacrylate) (PLMA)).

$CsPbBr_3/AlO_x$: Loiudice et al. used atomic layer deposition (ALD) to synthesize $CsPbBr_3/AlO_x$ nanocomposites. PQDs were spin-coating on glass substrate. Then, trimethylaluminum (TMA) and H_2O were used as AlO_x precursors and were deposited on surface of PQDs. Given the highly compact protective layer, these $CsPbBr_3/AlO_x$ nanocomposites exhibited high stability against immersion in water and thermal treatment.

Even though formation of inorganic shell insulates at the surface of PQDs, it cannot maintain charge transport properties resulting in decreasing of device performance when applied to optoelectronic or photovoltaic applications.

Z. Li et al. demonstrated surface coating of $CsPbBr_3$ NCs with TiO_2 to improve stability in ambient air. TiO_2 shell coated $CsPbBr_3$ NCs were synthesized through the encapsulation of colloidal $CsPbBr_3$ NCs with titanium precursor, then, calcined at 300 °C. TiO_2 shell coating show excellent water stability for at least three months. More importantly, $CsPbBr_3$/TiO_2 not only improves the stability of PQDs but also exhibits increase in charge separation efficiency due to the electrical conductivity of the TiO_2 shell. [13]

2.6   PQDs purification process and thin-film fabrication

The synthesized PQD crude solutions generally certain amount of impurities such as n-octadecene, oleic acid, and oleylamine. These impurities act as an electrical insulator that inhibits charge carrier injection or transport in optoelectronic or photovoltaic device.

J. Li et al. reported purification process of PQDs using reprecipitation method (figure 2.12a). The synthesized PQDs surrounded by long chain organic ligand were dispersed in non-polar solvents such as toluene, octane, and hexane. These solvents have low dielectric constants, and they act as good solvents in the reprecipitation process. On the other hand, polar solvents with high dielectric constants were used as poor solvents such as butanol (BuOH) and ethyl acetate (AcOEt). When the poor solvents were added to PQDs dispersed in a good solvent, they allow precipitation and isolation of PQDs by centrifugation. The impurities containing supernatant was discarded to remove impurities. However, PQDs are very sensitive to polar solvent, causing decomposition of the perovskite structure leading to the optical quenching.

K. Hoshi demonstrated the purification process of $CsPbBr_3$ PQDs without optical quenching using low dielectric-constant solvents such as dimethyl ether (ε = 7.23) to completely remove impurities. 36 different solvents were studied, as shown in figure 2.12a, the results show that the appropriate choice of poor solvents used to remove surface ligand without quenching of PQDs is the solvent with dielectric constants less than 10 (ε<10). [33]

J. Li et al. reported the systematic purification process of $CsPbBr_3$ QDs for achieving high-efficiency LEDs using the poor solvent ethyl acetate which has low dielectric constant (ε = 6.02). The presence of impurities was confirmed by proton nuclear magnetic resonance (H-NMR) measurement. The completely removal of octadecene was observed with increasing reprecipitation cycles. The green LED based on two-cycle reprecipitation $CsPbBr_3$ QDs reached the peak EQE of over 6%. [34]

These results suggested that appropriate choice of poor solvents and increasing reprecipitation cycle is significant for effective purification of PQDs. However, multiple wash processes before thin-film deposition can result in a strong aggregation and decreasing in QDs performance. In this case, purification process of PQDs after thin film deposition has been studied.

The first study of $CsPbI_3$ PQDs thin film fabrication method together with an effective ligand removal process using methyl acetate was reported by Swarnkar et al. in 2016. The resultant photovoltaic device showed PCE of 10.77% with open-circuit voltage of 1.23 V. The $CsPbI_3$ PQDs were deposited layer by layer and each QD layer was immersed into a saturated lead (II) nitrate $[Pb(NO_3)_2]$ solution in MeOAc to partially remove the native ligands and allow for further layers to be deposited without re-dispersing the exiting layers, as shown in figure 2.12c. [35]

Q. Zhao., et al., also reported layer-by-layer deposition of PQDs films and demonstrated ligand removal using MeOAc. A layer of QDs was deposited from the colloidal solution followed by ligand removal process, rendering the resulting film insoluble to the nonpolar solvent, enabling the ability to process the subsequent QD-layers without affecting the underlying film. [36]
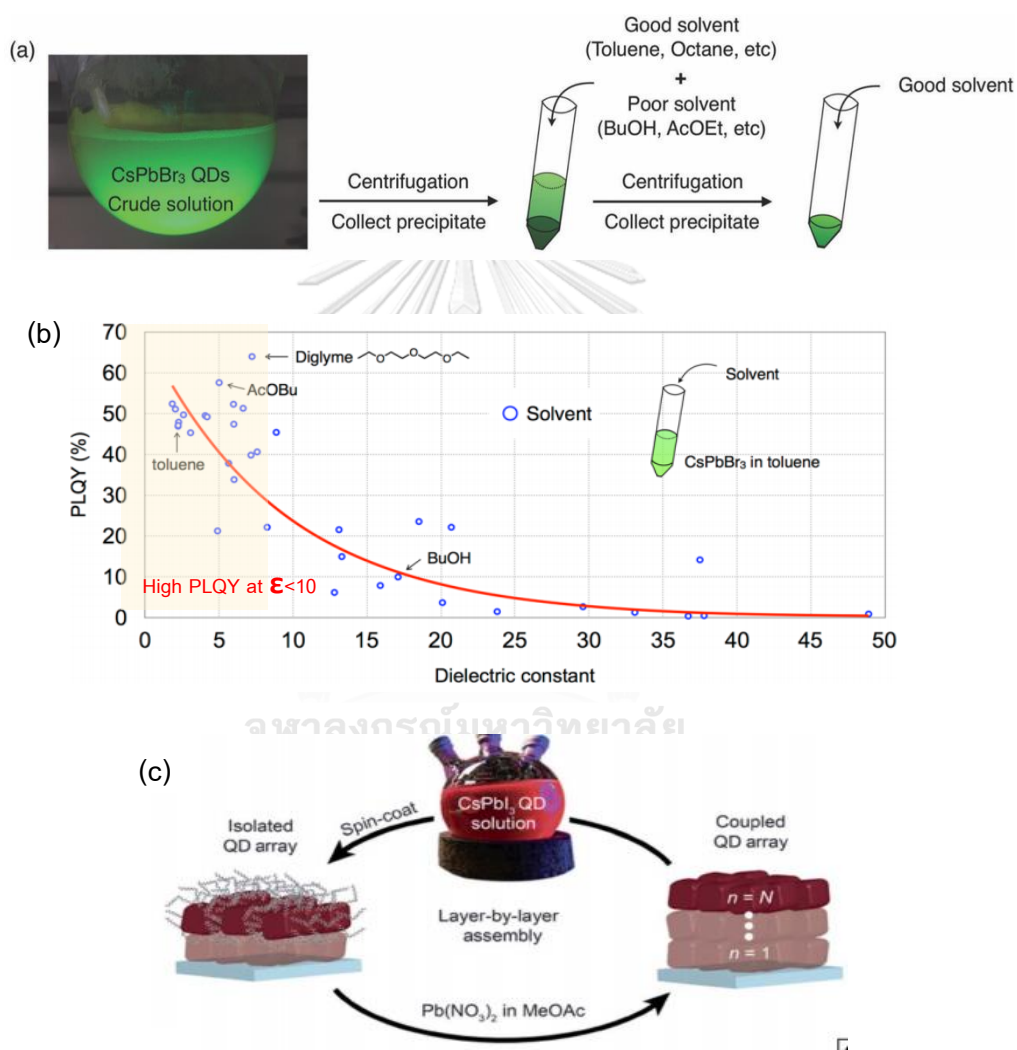
Figure 2. 12 (a) Ligand removal by reprecipitation method. [34] (b) Relationship between PLQY and the dielectric constants of various washing solvents. [33] (c) Schematic of the film deposition and post-treatment procedure. [35]

Therefore, in this work we perform a thin film fabrication method of $CsPbBr_3/TiO_2$ PQD by comparison of PQDs purification process consisting of a simple reprecipitation and layer by layer deposition using same washing solvent, MeOAc, to produce high uniformity and optical properties of $CsPbBr_3/TiO_2$ QD film. In addition, a colloidal $CsPbBr_3/TiO_2$ QDs dispersion in toluene are deposited on cleaned substrate by spin coating method.

2.7   Thin-film fabrication

2.7.1   Spin coating technique

Spin coating technique is widely used for thin film fabrication to deposit uniform coating of organic materials on flat surfaces. Spin coating is divided in four steps including deposition, spin up, spin off, and evaporation, as shown in figure 2.13. In the first step, the material is dropped on the turntable and then spin up and spin off occurring in sequence while the evaporation stage occurs throughout the process. The solution is distributed via centrifugal force. Thinning of the layers resulted from high spinning speed, followed by drying of the applied layer. The rapid rotation causes uniform evaporation of the solvent. High volatile components are removed from the substrate because of the evaporation or simply drying and the low volatile components of the solution remain on the surface of the substrate. Thickness of the deposited layer is controlled by the viscosity of the coating solution and the speed of rotation. [37]
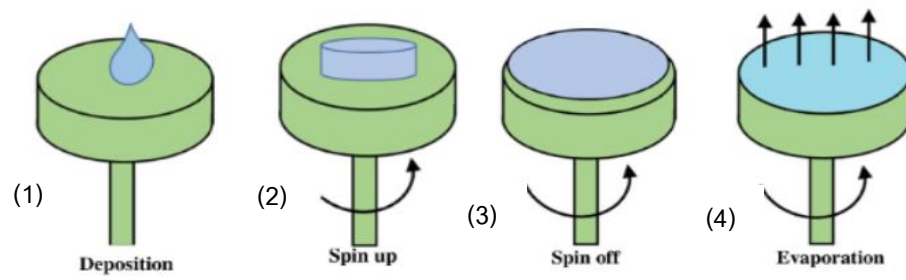
Figure 2. 13 Spin coating steps. [37]

CHAPTER III

EXPERIMENT

This chapter describes the experimental procedures for materials and $CsPbBr_3/TiO_2$ thin film deposition method which were divided into three parts including synthesis of $CsPbBr_3/TiO_2$ QD composite, ligand removal process, and perovskite solar cell device fabrication. The experimental procedures were described as follow:

3.1   Materials

3.1.1   Chemicals

1)   Lead bromide ($PbBr_2$, >98%, Tokyo chemical industry)

2)   Cesium carbonate (Cs_2CO_3, 99.99%, Tokyo chemical industry)

3)   Lead acetate ($Pb(CH_3COO)_2 \cdot 3H_2O$, 99.99%, Tokyo chemical industry)

4)   Benzoyl bromide (C_6H_5COBr, 98%, Tokyo chemical industry)

5)   Oleic acid (OA, >65%, FUJIFILM wako pure chemical)

6)   Oleylamine (OAm, 70%, FUJIFILM wako pure chemical)

7)   1-octadecene (1-ODE, 95%, FUJIFILM wako pure chemical)

8)   Toluene (≥99.3%)

9)   Titanium tetraisopropoxide ($Ti[OCH(CH_3)_2]_4$, 95%, FUJIFILM wako pure chemical)

10)   Methyl acetate (MeOAc, 95%, FUJIFILM wako pure chemical)

3.1.2   Equipment

1)   Vacuum line

2)   Hot plate stirrer

4)   Centrifuge

5)   Spin coater

6)   UV-Vis Spectrophotometer

7)   X-ray diffractometer

8)   DLS spectrophotometer

9)   Photoluminescence spectrometer

10)   Transmission electron microscope

11)   Scanning electron microscope

3.2   Experimental

3.2.1   Synthesis of $CsPbBr_3/TiO_2$ QD composite

$CsPbBr_3/TiO_2$ QD composite was synthesized by hot-injection. 16 mg of cesium carbonate (Cs_2CO_3), 76 mg of lead acetate trihydrate ($Pb(CH_3COO)_2 \cdot 3H_2O$), 0.45 mL of oleic acid (OA), 1 mL of oleylamine (OAm), and 5 mL of 1-octadecene (ODE) were loaded into 50 mL three-neck flask, respectively. The mixed solution was dried under vacuum at 130 °C for 1 h and heated to 170 °C under a flow of argon gas. Then, 72 µL of benzoyl bromide, as a bromide precursor, was quickly injected into the mixed solution followed by 60 µL of titanium tetraisopropoxide, as a titanium precursor. The mixed solution was then immediately cooled down in ice-water bath and wait until the temperature decreased to room temperature. The crude solution was then centrifuged at 4000 rpm for 10 min to remove excess ligand. The precipitates were collected and re-dispersed in 5 mL toluene for further use.

3.2.2 Ligand removal process

The CsPbBr$_3$/TiO$_2$ QD composite dispersed in toluene from the previous step was washed with the removal solvent several times in order to remove the surface ligands. The procedures were started by addition of 15 mL of methyl acetate, which acts as a removal solvent, into the QD dispersion followed by centrifugation at 8000 rpm for 5 min. The precipitation was collected and then re-dispersed again in toluene. These processes were repeated until 3 times to remove almost all amount of ligands.

3.2.3 Perovskite solar cell fabrication

1) Substrate cleaning

The FTO coated glasses were used as a substrate for the solar cell device, which acts as a transparent electrode of the solar cell. The FTO coated glass substrates were cleaned by soaking in the mixture of 20 mL of hydrogen peroxide, 20 mL of ammonia, and 100 mL of DI water followed by heating up to 70 °C for 10 min. Then, the substrates were cleaned with DI water and acetone, respectively. Finally, the washed substrates were treated by UV-O$_3$ for 15 min before thin-film deposited.

2) Deposition of perovskite solar cell

The perovskite solar cells were fabricated on FTO glass substrates with the device configuration: FTO/perovskite QD/gold electrode, as shown in **figure 3.1.** Firstly, the washed CsPbBr$_3$/TiO$_2$ QD composite dispersion was deposited on the cleaned FTO glass substrate by spin coating technique. 60 µL of the washed CsPbBr$_3$/TiO$_2$ QD composite dispersion was dropped into cleaned FTO glass substrate followed by spun up the spin coater to deposit the film with the spin

coating rate of 3000 rpm and time of 20 s to obtain the $CsPbBr_3/TiO_2$ QD film. Then, gold electrode was deposited on to the perovskite QD active layer by thermal evaporation technique to complete the entire structure of solar cell device.

3.3 Characterization

3.3.1 $CsPbBr_3/TiO_2$ QD composite characterizations

1) The crystal structure of the obtained $CsPbBr_3$ and $CsPbBr_3/TiO_2$ QDs was examined by X-ray diffraction (XRD).

2) Light absorption spectra of the obtained $CsPbBr_3$ and $CsPbBr_3/TiO_2$ were measured by UV-vis spectroscopy.

3) Light emission spectra of the obtained $CsPbBr_3$ and $CsPbBr_3/TiO_2$ were measured by photoluminescence (PL) measurement.

4) The crystalize size and formation of TiO_2 shell coated $CsPbBr_3$ were measured by transmission electron microscopy (TEM).

3.3.2 Ligand removal process characterizations

1) The washed solution was then characterized by FTIR to confirm removal of surface ligands.

2) The effect of washing solvent to optical properties of $CsPbBr_3/TiO_2$ including absorption spectra was characterized by UV-vis spectroscopy.

3) The smoothness and morphology of the obtained films prepared from different samples were observed under UV light irradiation.

3.3.3 Perovskite solar cell fabrication characterizations

1)   The morphology and thickness of perovskite thin films were observed by using scanning electron microscopy (SEM).

2)   The solar cell performance parameters, including photocurrent density-voltage (J-V) curve, open circuit voltage (V_{oc}), Fill factor (FF), and power conversion efficiency (PCE) of the obtained perovskite quantum dot solar cell devices were calculated from the current-voltage characteristic measurement.

CHAPTER IV

RESULT AND DISCUSSION

The synthesis of $CsPbBr_3$/am-TiO_2 QD composite was performed by a simple method. Firstly, the formation of TiO_2 on $CsPbBr_3$ QD and effects of TiO_2 coating on the optical properties of $CsPbBr_3$ QD were observed. Afterwards, the preparation of $CsPbBr_3$/am-TiO_2 QD composite as an active layer for solar cell device was performed. Perovskite QD are generally surrounded by long chain organic ligands hindering charge transport properties, therefore, these long chain organic ligands need to be removed before applying these materials for solar cell application. The effects of ligand removal process using methyl acetate as a removal solvent on optical properties of $CsPbBr_3$/am-TiO_2 QD composite were investigated. Finally, the deposition of $CsPbBr_3$/am-TiO_2 QD composite as an active layer on solar cell device was performed using spin coating technique and the solar efficiency of the device was determined which was also compared to the bare $CsPbBr_3$ QD device. The results and discussions can be divided into four parts as follows,

4.1   Synthesis of $CsPbBr_3$/TiO_2 composite

$CsPbBr_3$ QDs were synthesized by hot-injection and coated with TiO_2 by injection of titanium tetraisopropoxide (TTIP) as a TiO_2 precursor into $CsPbBr_3$ crude solution during the formation of $CsPbBr_3$ QDs to form $CsPbBr_3$/TiO_2 QD composite. The XRD diffraction of $CsPbBr_3$/TiO_2 QD composite and $CsPbBr_3$ NCs presented in **figure 4.1A** shows peaks at 15°, 21.5°, 31°, 34°, and 38° corresponding to the $CsPbBr_3$ crystal structure. However, the XRD pattern exhibits similar Bragg's angles for intense peaks to both orthorhombic and cubic phase of $CsPbBr_3$ which is difficult to distinguish. It was clearly seen that the splitting peak at 31° of $CsPbBr_3$ NCs is similar to the orthorhombic phase of $CsPbBr_3$ which is

different to the $CsPbBr_3/TiO_2$ QD composite which shows only one peak at the same degree. This could be concluded that the $CsPbBr_3$ QDs are in orthorhombic phase, and due to the $CsPbBr_3/TiO_2$ QD composites, which were synthesized using the same, therefore, $CsPbBr_3/TiO_2$ should have the same crystallinity as orthorhombic as $CsPbBr_3$.
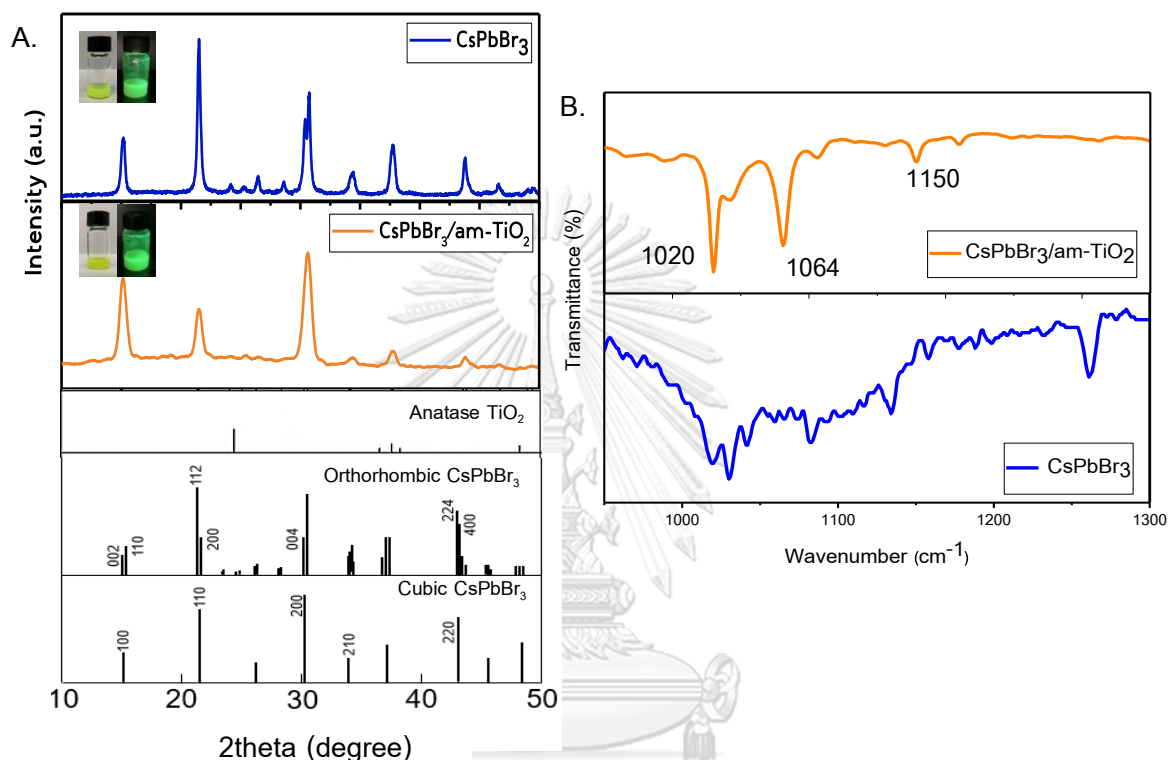
Figure 4. 1 (A) XRD pattern of $CsPbBr_3$ and $CsPbBr_3/TiO_2$; the insets are images of colloidal QD in normal light (left) and 365 nm UV light (right), and (B) The FTIR spectrum of $CsPbBr_3/TiO_2$ QD composite, and $CsPbBr_3$ QD.

Considering the XRD pattern of $CsPbBr_3/TiO_2$ QD composite, the XRD peak ascribed lattice planes of crystalline TiO_2 cannot be observed due to the phase formation at high temperature of more than 300 °C to transfer from amorphous phase to crystalline TiO_2. This is possible that TiO_2 was formed with $CsPbBr_3$ QD by bonding of amorphous TiO_2 (am-TiO_2) with QD due to the addition of TiO_2 precursor during the formation of $CsPbBr_3$ QD. The presence of am-TiO_2 resulted in the change in molecular interaction of $CsPbBr_3$ QD and molecular structure to be distorted which was observed from the

decreasing of XRD peak intensity of $CsPbBr_3$/am-TiO_2 QD composite at 2θ equal to $21.5°$ corresponding to 112 and 200 lattice planes of $CsPbBr_3$ QD. However, there is no shift in peak position.

The FTIR spectra of $CsPbBr_3$/am-TiO_2 QD composite in **figure 4.1B** shows peak in the 1020 - 1150 cm^{-1} region close to the vibration of Ti-O- [13] which was not observed from bare $CsPbBr_3$ QD. Nevertheless, the hydroxyl groups (O-H) and Ti-O bond should be examined by X-ray photoelectron spectroscopy (XPS) to confirm the hydrolysis reaction of TiO_2 and the formation of amorphous TiO_2.

The crystallite size of $CsPbBr_3$ was estimated to be 12.65 nm from Scherrer's equation. After coating with am-TiO_2, the crystallite size of the $CsPbBr_3$/am-TiO_2 QD composite was increased to 13.30 nm. This could be attributed to the incorporation of am-TiO_2 in the perovskite structure.

Figure 4.2 presents the TEM images of the $CsPbBr_3$ QD (**figure 4.2A**) and $CsPbBr_3$/am-TiO_2 QD composite (**figure 4.2B**), which can confirm the estimated average crystallite size of 12.18 nm for $CsPbBr_3$ and 13.24 nm for $CsPbBr_3$/am-TiO_2 QD composite. Moreover, the TEM image shows broader particle size distribution of $CsPbBr_3$/am-TiO_2 QD composite because the increasing of reaction time by stirring for 2 h after addition of TiO_2 precursor for hydrolysis reaction this caused the agglomeration of QD to form the larger particle size. However, these larger particles were eliminated by filtration before QD thin film deposition. For the TEM images of $CsPbBr_3$/am-TiO_2 QD, it was found that many small amounts of am-TiO_2 were grown, observed from the dark dot inside the particles of $CsPbBr_3$ forming the heterostructure $CsPbBr_3$/am-TiO_2 QD composite which was not observed from the TEM image of $CsPbBr_3$. Nevertheless, the formation and distribution of am-TiO_2 within the QD particles should be further analyzed by High-resolution TEM (HRTEM) and Elemental dispersive X-ray (EDX) mapping analysis.
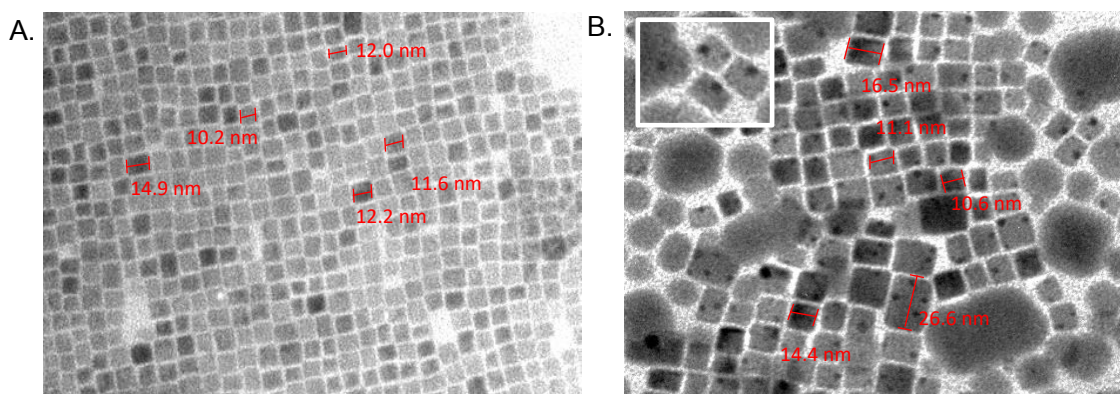
Figure 4. 2 TEM images of (A) CsPbBr$_3$ QD, (B) CsPbBr$_3$/am-TiO$_2$ QD composite.

4.2 Effect of TiO$_2$ coating on optical properties of CsPbBr$_3$ QD

The optical properties of the CsPbBr$_3$/am-TiO$_2$ QD composite prepared by hot-injection were studied to investigate the suitability for solar cell application. **Figure 4.3A** shows PL emission and UV-visible light absorption spectra of CsPbBr$_3$ with and without TiO$_2$ coating. It was found that the PL emission intensity decreased after coating with TiO$_2$. This could be influenced from various possible reasons including the generation of defect level as trap states for photogenerated charge carriers [38, 39], the change of CsPbBr$_3$ perovskite structure after TiO$_2$ coating, and electron transfer from CsPbBr$_3$ to TiO$_2$ resulting in PL quenching in CsPbBr$_3$/TiO$_2$ QDs [40]. The electron transfer can be further confirmed by apply to solar cell device and photoelectrochemical cell to measure the photo-response of this material.

In addition, the PL emission spectra of CsPbBr$_3$ shows emission wavelength at 517 nm and there is no change in PL emission wavelength after am-TiO$_2$ coating. The PL emission wavelength relates to the bandgap energy of QD suggesting that am-TiO$_2$ coating by addition of TTIP during the formation of CsPbBr$_3$ QD has no effect on bandgap energy of QD. However, the decreasing of energy bandgap was observed from Tauc's plot in **figure 4.3B** from 2.25 eV of CsPbBr$_3$ to 2.11 eV of CsPbBr$_3$/am-TiO$_2$ QD composite

which could be influenced from the quantum confinement effect by increasing of the particle size due to the incorporation of am-TiO$_2$ with CsPbBr$_3$ QD particle. The slightly decreased in bandgap of about 0.14 eV resulted from the slightly increased in particle size of about 0.65 nm after am-TiO$_2$ coating. However, these slightly changing did not significantly affects on changing in PL emission wavelength.
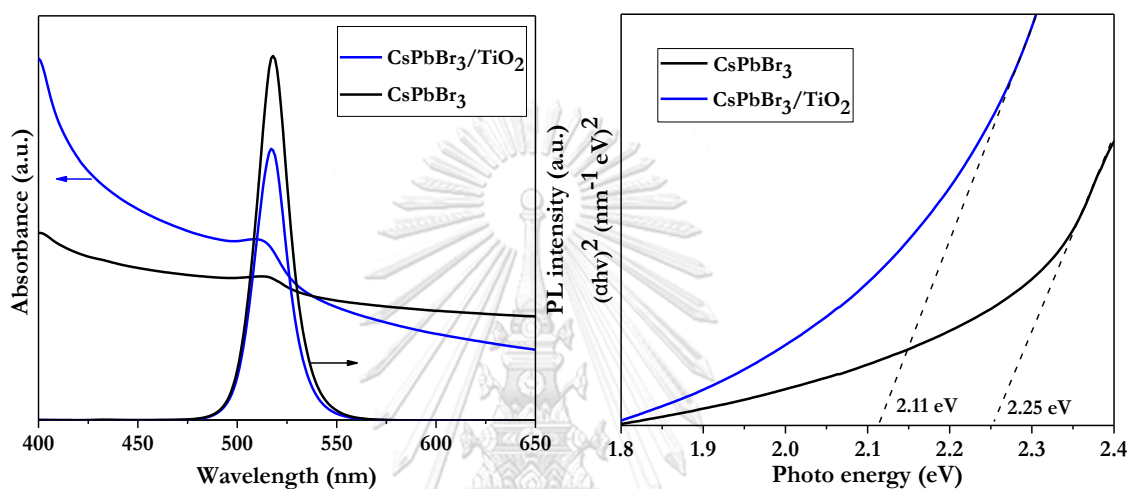
Figure 4. 3 (A) PL emission and UV-visible light absorption spectra of CsPbBr$_3$ and CsPbBr$_3$/am-TiO$_2$ QD composite dispersion in toluene, (B) Tauc's plot of CsPbBr$_3$ and CsPbBr$_3$/am-TiO$_2$ QD composite

Moreover, am-TiO$_2$ coating shows the effect on light absorption ability determined by UV-visible spectroscopy as shown in **figure 4.3A**. The results show the light absorption wavelength of CsPbBr$_3$ and CsPbBr$_3$/TiO$_2$ in the visible light region and the band edge energy at about 513 nm. Moreover, the light absorption ability of CsPbBr$_3$/TiO$_2$ slightly increased in the wavelength lower than 513 nm approaching to UV region which was attributed to absorption ability of amorphous TiO$_2$. These results could be concluded that the introduction of am-TiO$_2$ can facilitate charge separation, hinder charge recombination, and enhance light absorption ability in the UV-visible region. These properties can be used in optoelectronic and photovoltaic applications.

4.3 Ligand removal process

In general, perovskite QDs are surrounded by long chain organic ligands. A presence of ligands prevents an efficient charge carrier injection in solar cell device, therefore which needs to be removed. Herein, we demonstrate the ligand removal process using a removal solvent by mixing non-polar solvent (toluene) which was used to maintain QD colloidal stability with higher polarity solvent (methyl acetate, MeOAc) to extract the surface ligands from perovskite QD while maintaining their structure.

The FTIR spectra of colloidal $CsPbBr_3$/am-TiO_2 QD composite before washing (labeled as SP0) and after 1 (SP1), 2 (SP2), and 3 (SP3) times washing with ligand removal solvent are shown in **figure 4.4A**. The FTIR spectra in 2800 – 3100 cm^{-1} range, **figure 4.4C**, shows the vibrational modes of hydrocarbon chain of oleic acid and oleylamine. The peaks at 2917 cm^{-1} and 2850 cm^{-1} ascribed the intense symmetric and antisymmetric C-H stretching of methylenic groups and 2960 cm^{-1} attributed to the antisymmetric stretching of the terminal -CH_3 group. [41] The decreasing of FTIR peak intensity in 2800 – 3100 cm^{-1} range was observed upon the increasing of washing cycle up to 3 times indicating the removal larger amount of surrounded organic surface ligand. The FTIR spectrum at 1350 - 1700 cm^{-1} region, **figure 4.4B**, mainly dominated by the intense peak at 1459 cm^{-1} corresponding to the –CH_2 group and almost all of this group was observed to be mainly removed due to the decreasing of FTIR peak intensity by increasing the washing cycle. However, the peak at 1463 cm^{-1} was still observed after 3 times washing corresponding to the –CH_2– bending of the hydrocarbons chain which still remains on the surface of QD. It can be concluded that larger amount of surface ligands could be removed upon the increasing the washing cycle, however, there are still have some of ligands remain on the QD surface. Nevertheless, the amount of surface ligand removed

upon the increasing of washing cycle should be quantitatively analyzed by thermogravimetric analysis (TGA).
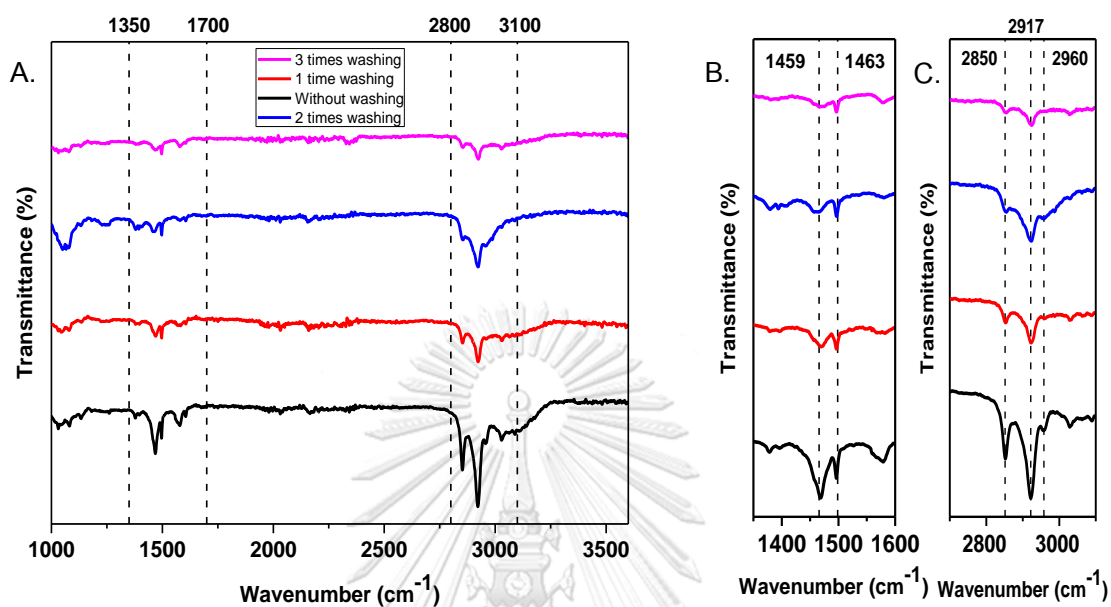
Figure 4. 4 (A) The FTIR spectra of colloidal $CsPbBr_3$/am-TiO_2 QD composite and the enlarge FTIR spectra, at (B) 1350 – 1700 cm^{-1} and (C) 2800 – 3100 cm^{-1} ranges, at different washing cycle.

In addition, the removal of large amount of surface ligands led to the loss in colloidal stability due to the generation of surface trap states. The ligand in free state can bond into the surface of another QD, resulting in the aggregation of QD, losing their optical properties, inferioring performance and also affecting the film formation. [42] Therefore, the effects of ligand removal process on the optical properties and QD film morphology were then investigated.

4.3.1   Effect of ligand removal on optical property

The effect of washing cycles on light absorption spectra was examined by UV-visible spectroscopy. The UV-visible light absorption spectra of $CsPbBr_3$/am-TiO_2 QD composite with different number of washing times are showed in **figure 4.5A**. The light absorption spectra show no change in light absorption band edge at 514 nm indicating that the increasing of washing cycles has no effect on light absorption wavelength of QD. However, a decrease in light absorption in the wavelength of 514-700 nm was observed. This resulted from a decrease in bandgap which could be attributed to the increase in particle size due to the aggregation of QD by increasing number of washing cycles.

The estimated bandgap values of each sample were examined by Tauc's plot, as shown in **figure 4.5B,** and summarized in **table 4.1**. It was confirmed that the bandgap values decreased from 2.43 eV of QD without washing to 2.16 eV of QD with 3 times washing. The narrower bandgap can harvest a wider range of sunlight which is beneficial for solar cell application.
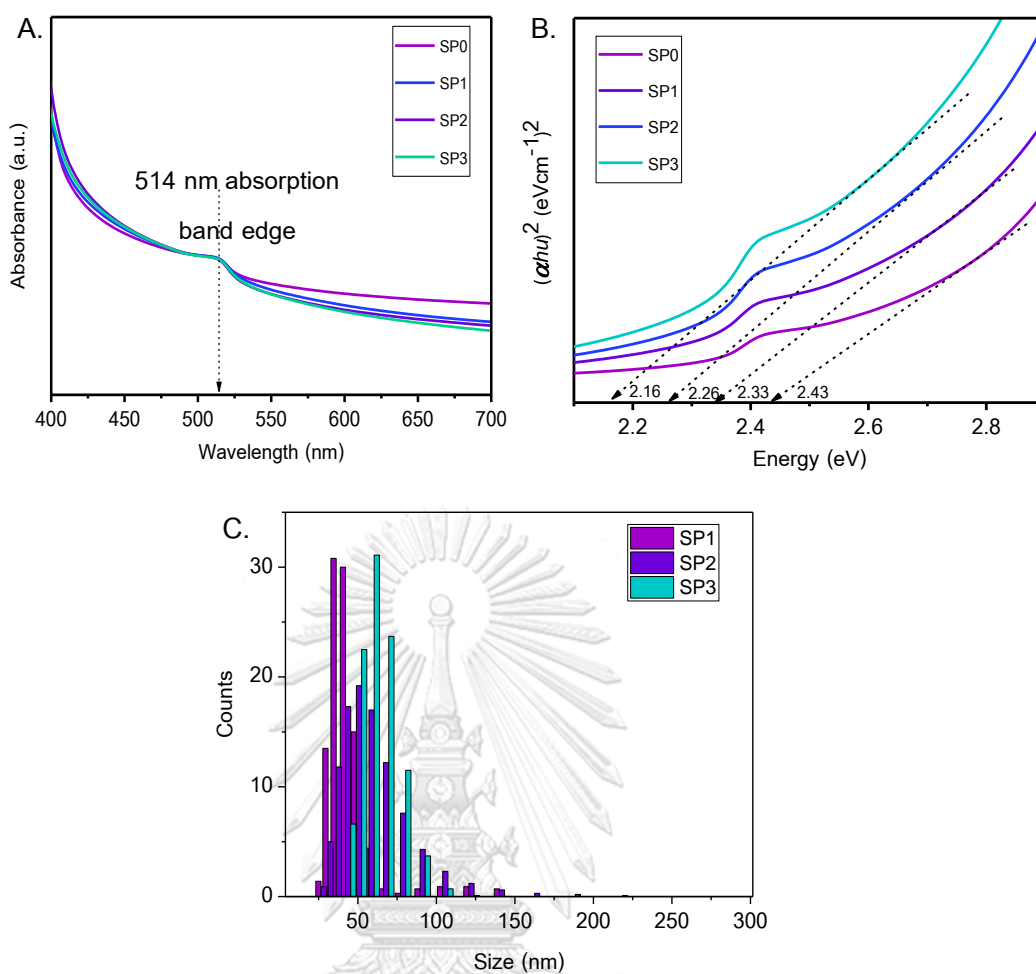
Figure 4. 5 (A) UV-visible light absorption spectra, (B) Tauc's plot, (C) particle size distribution of CsPbBr$_3$/am-TiO$_2$ QD composite at different number of washing times.

Table 4. 1 The energy band gaps of CsPbBr$_3$/am-TiO$_2$ QD composite at difference number of washing times.

Samples	Energy band gap (eV)
No washing (SP0)	2.43
1 time washing (SP1)	2.33
2 times washing (SP2)	2.26
3 times washing (SP3)	2.16

4.3.2 Effect of ligand removal on crystallite size and film morphology

Figure 4.6 demonstrates digital images of spin coated QD thin films prepared from colloidal QDs with different number of washing cycles. These QD thin films were observed under UV light excitation. Increasing the washing cycles resulted in the bad film morphology due to a larger amount of surface defects, which could be attributed to the serious loss of surface ligands resulting in the aggregation of QD and broader particles size distribution. The Dynamic light scattering (DLS) analysis in **figure 4.5C** confirmed the increasing particle size and particles size distribution after increasing the number of washing times. The estimated average particle size of each samples was summarized in **table 4.2**. However, it can be found that the QD film morphology and uniformity can be preserved very well in the first two cycles, and clearly seen the creation of film defects after 3 cycles of washing attributed to the formation of the larger particles size. The thin film quality is very crucial for the final film performance because the film with more defects will greatly affect the charge transport within solar cell device. To summarize the ligand removal process, 2 cycles of washing can remove large amount of surface ligands (from FTIR) and shows less effect on thin film uniformity and suitable bandgap for solar cell application. These are the optimal conditions for ligand removal process of $CsPbBr_3$/am-TiO_2 QD composite before deposition as a thin film for solar cell device.

Table 4. 2 The average particles size of $CsPbBr_3$/am-TiO_2 QD composite at difference number of washing times.

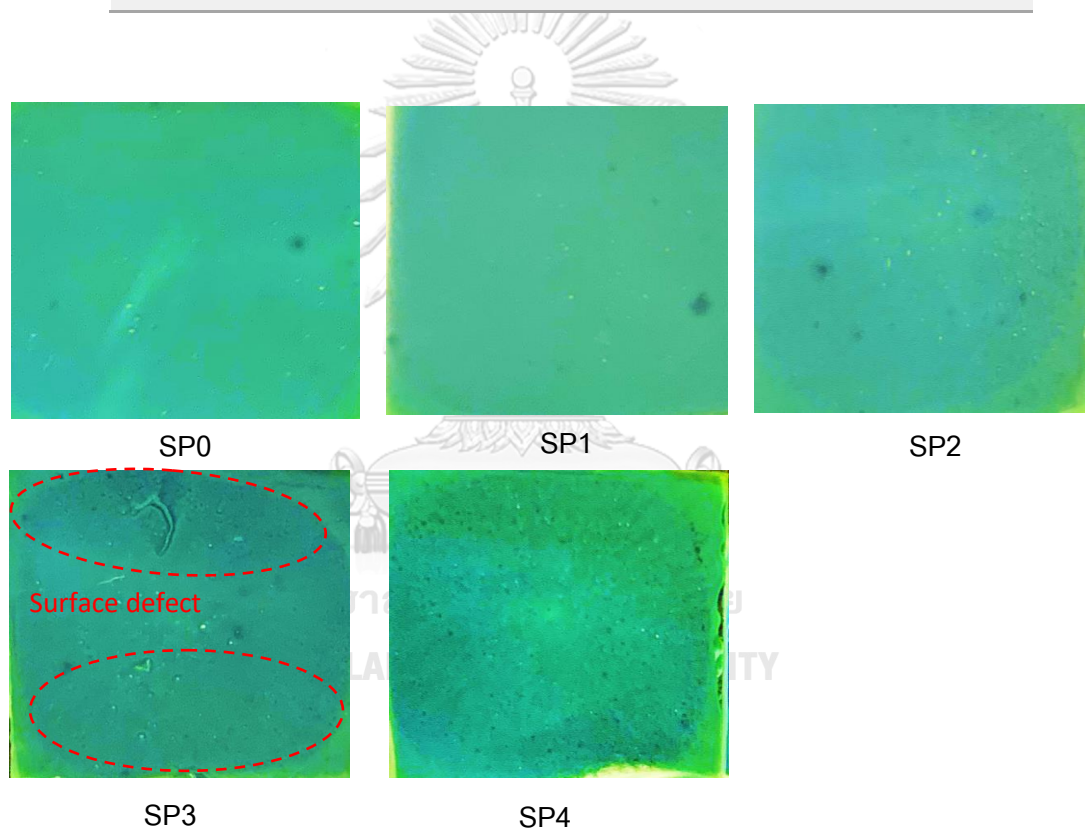| Samples	Average particles size (nm)
1 time washing (SP1)	42
2 times washing (SP2)	47
3 times washing (SP3)	62

SP0   SP1   SP2

SP3   SP4

Surface defect

Figure 4. 6 The digital images of $CsPbBr_3$/am-TiO_2 QD composite thin film at different washing cycles.

4.4   Solar cell device fabrication

In order to confirm the enhancement of the charge separation properties of CsPbBr$_3$ QD by coating with am-TiO$_2$. The obtained CsPbBr$_3$/am-TiO$_2$ QD composite was applied as an active layer for solar cell device and compared to the device using bare CsPbBr$_3$ as an active layer. **Figure 4.7A and B** present the surface and cross-sectional FE-SEM images of the spin-coated CsPbBr$_3$/am-TiO$_2$ QD film on FTO coated glass substrate, respectively. The images show uniform and compact film with the thickness of 14,000 nm for CsPbBr$_3$/am-TiO$_2$ layer. The film thickness has an influence on the cell efficiency because thicker film serves the greater resistance to charge transport, it needs to be further study to investigate the optimal thickness for solar cell device.
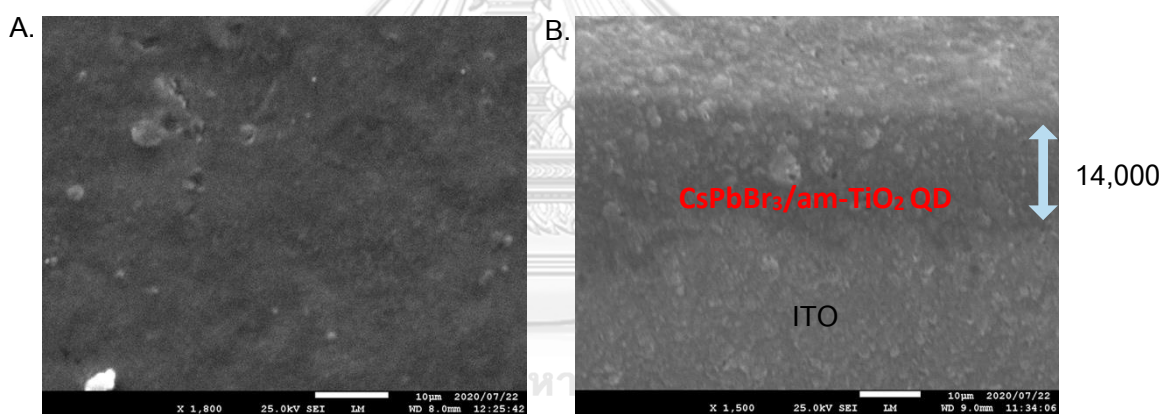
Figure 4. 7 (A) The surface, (B) Cross-section FE-SEM images of CsPbBr$_3$/am-TiO$_2$ QD thin film on FTO coated glass substrate.

The short circuit current-voltage (J-V) characteristics of CsPbBr$_3$ QD and CsPbBr$_3$/am-TiO$_2$ device were measured under dark and light illumination, as shown in **figure 4.8A, and B**, respectively. It can be found that the current increases upon light illumination in both cases because of the photogenerated charge carriers by photon absorption of perovskite active layers. The champion current density of CsPbBr$_3$ QD and CsPbBr$_3$/am-TiO$_2$ films are 0.06 and 0.18 µA/cm^2, respectively. About 3 times

enhancement of photocurrent could be attributed to the enhancement of visible light absorption property of CsPbBr$_3$/am-TiO$_2$ QD composite and good charge separation property due to the generation of defect level inside the band gab as a pathway to extract charge carriers from CsPbBr$_3$ QD and reduce the recombination of the photogenerated electron hole pairs in device, as shown in **figure 4.7C,**

Figure 4. 8 The J-V characteristics in dark and light illumination of (A) CsPbBr$_3$ QD, (B) CsPbBr$_3$/am-TiO$_2$ nanocomposite., (C) Schematic representation the generation of defect level and electrons extraction pathway in QD particle., (D) The J-V curve of CsPbBr$_3$ and CsPbBr$_3$/am-TiO$_2$ QD device.

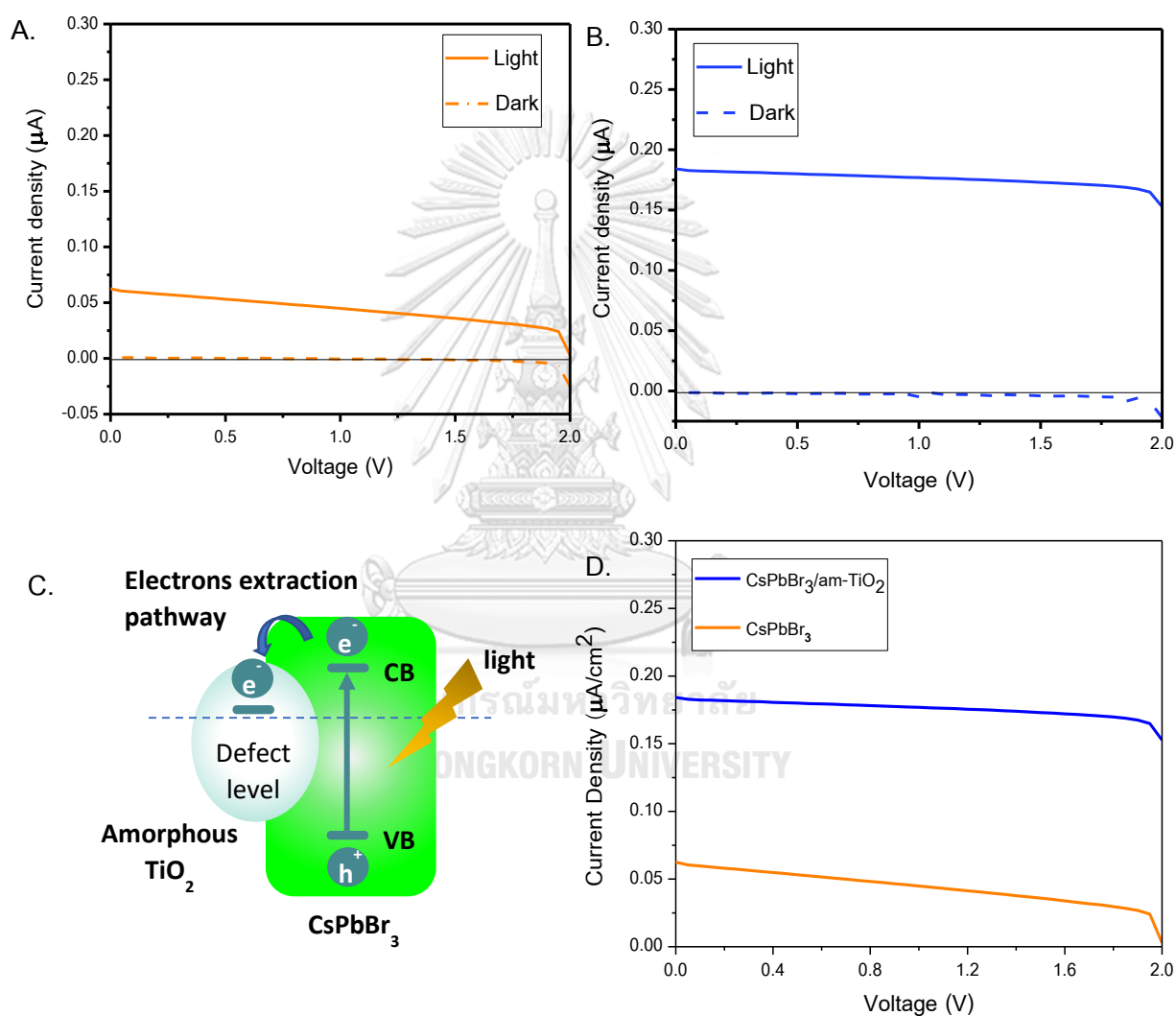The photovoltaic parameters including open-circuit voltage (V_{oc}), short-circuit current (J_{sc}), fill factor (FF), shunt resistance (R_{sh}), and the device performance represented by PCE values of $CsPbBr_3$ QD and $CsPbBr_3$/am-TiO_2 films were shown in **table 4.3**. The fill factor of $CsPbBr_3$ QD film was calculated to be 37.36% from J_{sc} of 0.06 $\mu A/cm^2$, V_{oc} of 2 V, and maximum power (P_{max}) of 0.32 μW, which shows lower efficiency compared to the $CsPbBr_3$/am-TiO_2 QD film. The $CsPbBr_3$/am-TiO_2 QD device shows a high fill factor up to 87.7% from 0.18 $\mu A/cm^2$ of J_{sc}, 2 V of V_{oc}, and 0.05 μW of P_{max}. Moreover, the shunt resistance (R_{sh}) of QD films were calculated to be 0.79 of CsPbBr3 film and 0.25 of $CsPbBr_3$/am-TiO_2 film.

Table 4.3 The performance of $CsPbBr_3$ and $CsPbBr_3$/am-TiO_2 QD films.

Samples	J_{sc} (μA)	V_{oc} (V)	Fill Factor	Shunt resistance (R_{sh})	PCE (%)
$CsPbBr_3$	0.06	2.0	37.36	0.79	0.00005
$CsPbBr_3$/am-TiO_2 QD composite	0.18	2.0	86.43	0.25	0.00032

The lower fill factor of $CsPbBr_3$ QD film can be resulted from the higher shunt resistance compared to the $CsPbBr_3$/am-TiO_2 film. The presence of shunt resistance causes the power loss in cell which are typically due to surface defects or the recombination of photogenerated electron hole pairs in the cell. Finally, the PCE of the device was calculated to be 0.00005 % of $CsPbBr_3$ based device and increased to be 0.00032 % of $CsPbBr_3$/am-TiO_2 QD device suggesting the higher charge transport property of the $CsPbBr_3$/am-TiO_2 QD based solar cell device. As a result, the performance of solar cell based on $CsPbBr_3$/am-TiO_2 QD composite film shows higher efficiency than

that of bare $CsPbBr_3$ QD based solar cell, due to the enhancement of light absorption and charge separation property from the presence of am-TiO_2. Therefore, the recombination of photogenerated electron hole pairs in the device can be reduced. In addition, due to a very low photocurrent measured from the film (in μA), the electron and hole transporting layer, which are typically present in the perovskite solar cell device, should be added to get higher solar cell efficiency.

Moreover, perovskite quantum dot thin layer was deposited by spin coating under ambient condition, this process causes the evaporation of non-polar solvent (toluene) which was used to maintain QD colloidal stability therefore QD film was exposed directly to moisture and oxygen in ambient air resulting in QD film degradation. Moreover, very high temperature (500 $^{\circ}$C) was used for gold electrode deposition by thermal evaporation technique. This process could be one of the reasons for QD film degradation. Because perovskite QD is sensitive to moisture, oxygen, and high temperature. It is possible that perovskite QD decomposes during thin film deposition processes which greatly affects the solar cell performance.

CHAPTER V

CONCLUSION

5.1 Conclusions

1. $CsPbBr_3$/am-TiO_2 QD composite was successfully synthesized via hot-injection by injection of TTIP as a TiO_2 precursor and the reaction time of 2 h. The TiO_2 was formed inside the perovskite structure in amorphous phase, which was confirmed by FTIR spectra and TEM images.

2. The effects of the TiO_2 coating on optical properties of $CsPbBr_3$ were investigated. The enhancement of the charge separation property of QD was expected by coating with TiO_2, which was determined by PL measurement. $CsPbBr_3$/am-TiO_2 composite also served the enhancement of light absorption in the visible region analysed by UV-visible light absorption spectra.

3. The optical bandgap of $CsPbBr_3$ was influenced by the am-TiO_2 coating. The energy bandgap of $CsPbBr_3$/am-TiO_2 QD composite was slightly decreased from 2.25 eV of $CsPbBr_3$ to 2.11 eV. Therefore, the bandgap energy of QD was not significantly changed after coating with am-TiO_2.

4. The effects of ligand removal process by increasing the number of washing times with the removal solvent were performed. It was found that almost all of the surface ligands were removed after 3 times of washing with methyl acetate, indicating that larger amount of surface ligands was removed by increasing washing cycles. By the way, more surface defects were generated from the losing of surface ligands leading to the aggregation of QDs forming the larger particles size. This is significantly influence on the film morphology by

increasing of film defects, which was clearly seen on the film that was prepared from the colloidal QDs with 3 times of washing cycles. However, the formation of larger particles size could decrease the bandgap energy due to the quantum confinement effect, which shows the beneficial for solar cell device. The 2 times washing cycles could be the optimal number of times for washing because the large amount of surface ligands was removed but still had less effect on film morphology and the bandgap energy was decreased to be 2.26 eV.

5. The enhancement of the charge separation and charge transport properties of the $CsPbBr_3$/am-TiO_2 QD composite were examined from the J-V characteristic of $CsPbBr_3$/am-TiO_2 QD composite based solar cell. The best power conversion efficiency of the $CsPbBr_3$/am-TiO_2 QD composite based solar cell device is 0.00032%, which is about 6 times higher than that of solar cell device without am-TiO_2 coating. Moreover, we can get the very large fill factor (FF) based on $CsPbBr_3$/am-TiO_2 QD composite solar cell.

5.2 Recommendations for the future work.

Due to a very low photocurrent and the power conversion efficiency measured from the $CsPbBr_3$/am-TiO_2 QD composite-based solar cell (in µA), the electron and hole transporting layer which are typically presence in perovskite solar cell device should be added to get higher solar cell efficiency.

REFERENCES

1.   Azman, A.Y., et al. *Study of renewable energy potential in Malaysia*. in *2011 IEEE Conference on Clean Energy and Technology (CET)*. 2011.

2.   Awasthi, A., et al., *Review on sun tracking technology in solar PV system.* Energy Reports, 2020. **6**: p. 392-405.

3.   Yan, J. and B.R. Saunders, *Third-generation solar cells: a review and comparison of polymer:fullerene, hybrid polymer and perovskite solar cells.* RSC Advances, 2014. **4**(82): p. 43286-43314.

4.   Kojima, A., et al., *Organometal Halide Perovskites as Visible-Light Sensitizers for Photovoltaic Cells.* Journal of the American Chemical Society, 2009. **131**(17): p. 6050-6051.

5.   Yu, Z., A. Hagfeldt, and L. Sun, *The application of transition metal complexes in hole-transporting layers for perovskite solar cells: Recent progress and future perspectives.* Coordination Chemistry Reviews, 2020. **406**: p. 213143.

6.   Zhang, Y., et al., *Major Impediment to Highly Efficient, Stable and Low-Cost Perovskite Solar Cells.* Metals, 2018. **8**(11).

7.   Duan, J., et al., *Inorganic perovskite solar cells: an emerging member of the photovoltaic community.* Journal of Materials Chemistry A, 2019. **7**(37): p. 21036-21068.

8.   *Best Research-Cell Efficiency Chart.* The national renewable energy laboratory, 2019.

9.   Zhou, R., et al., *Synergistic combination of semiconductor quantum dots and organic-inorganic halide perovskites for hybrid solar cells.* Coordination Chemistry Reviews, 2018. **374**: p. 279-313.

10.   Shaikh, J.S., et al., *Quantum Dot Based Solar Cells: Role of Nanoarchitectures, Perovskite Quantum Dots, and Charge-Transporting Layers.* ChemSusChem, 2019. **12**(21): p. 4724-4753.

11.   Kong, X., et al., *Graphene/Si Schottky solar cells: a review of recent advances and prospects.* RSC Advances, 2019. **9**(2): p. 863-877.

12. Zheng, Z., et al., *Significantly improving the moisture-, oxygen- and thermal-induced photoluminescence in all-inorganic halide perovskite CsPbI3 crystals by coating the SiO2 layer*. Journal of Luminescence, 2019. **216**: p. 116722.

13. Li, Z.-J., et al., *Photoelectrochemically Active and Environmentally Stable CsPbBr3/TiO2Core/Shell Nanocrystals*. Advanced Functional Materials, 2018. **28**(1).

14. Chiba, T. and J. Kido, *Lead halide perovskite quantum dots for light-emitting devices*. Journal of Materials Chemistry C, 2018. **6**(44): p. 11868-11877.

15. Chiba, T., et al., *High-Efficiency Perovskite Quantum-Dot Light-Emitting Devices by Effective Washing Process and Interfacial Energy Level Alignment*. ACS Applied Materials & Interfaces, 2017. **9**(21): p. 18054-18060.

16. Moyen, E., et al., *Ligand removal and photo-activation of CsPbBr3 quantum dots for enhanced optoelectronic devices*. Nanoscale, 2018. **10**(18): p. 8591-8599.

17. Ling, X., et al., *14.1% CsPbI3 Perovskite Quantum Dot Solar Cells via Cesium Cation Passivation*. 2019. **9**(28): p. 1900721.

18. Olaleru, S.A., et al., *Perovskite solar cells: The new epoch in photovoltaics*. Solar Energy, 2020. **196**: p. 295-309.

19. Wang, F., X.-K. Liu, and F. Gao, *Chapter 1 - Fundamentals of Solar Cells and Light-Emitting Diodes*, in *Advanced Nanomaterials for Solar Cells and Light Emitting Diodes*, F. Gao, Editor. 2019, Elsevier. p. 1-35.

20. Musselman, K.P. and K. Poorkazem, *1 - Fundamental Understanding of Solar Cells*, in *Advanced Micro- and Nanomaterials for Photovoltaics*, D. Ginley and T. Fix, Editors. 2019, Elsevier. p. 1-17.

21. Ranabhat*, K., et al., *AN INTRODUCTION TO SOLAR CELL TECHNOLOGY*. iipp, 2016. **14(2016)4, 405**: p. 481 - 491

22. Ansari, M.I.H., A. Qurashi, and M.K. Nazeeruddin, *Frontiers, opportunities, and challenges in perovskite solar cells: A critical review*. Journal of Photochemistry and Photobiology C: Photochemistry Reviews, 2018. **35**: p. 1-24.

23. Zhou, Z., et al., *Interface engineering for high-performance perovskite hybrid solar cells.* Journal of Materials Chemistry A, 2015. **3**(38): p. 19205-19217.

24. Giovanni, D., *Optical-spin dynamics in organic-inorganic lead halide perovskites.* 2017.

25. Grätzel, M., *The light and shade of perovskite solar cells.* Nature Materials, 2014. **13**(9): p. 838-842.

26. Sumanth Kumar, D., B. Jai Kumar, and H.M. Mahesh, *Chapter 3 - Quantum Nanostructures (QDs): An Overview*, in *Synthesis of Inorganic Nanomaterials*, S. Mohan Bhagyaraj, et al., Editors. 2018, Woodhead Publishing. p. 59-88.

27. Protesescu, L., et al., *Nanocrystals of Cesium Lead Halide Perovskites (CsPbX3, X = Cl, Br, and I): Novel Optoelectronic Materials Showing Bright Emission with Wide Color Gamut.* Nano Letters, 2015. **15**(6): p. 3692-3696.

28. Eperon, G.E., et al., *Formamidinium lead trihalide: a broadly tunable perovskite for efficient planar heterojunction solar cells.* Energy & Environmental Science, 2014. **7**(3): p. 982-988.

29. Ogomi, Y., et al., *CH3NH3SnxPb(1–x)I3 Perovskite Solar Cells Covering up to 1060 nm.* The Journal of Physical Chemistry Letters, 2014. **5**(6): p. 1004-1011.

30. Hong, K., et al., *Low-dimensional halide perovskites: review and issues.* Journal of Materials Chemistry C, 2018. **6**(9): p. 2189-2209.

31. Deng, W., et al., *Organic-inorganic Hybrid Perovskite Quantum Dots for Light-Emitting Diodes.* Journal of Materials Chemistry C, 2018. **6**.

32. Huang, H., et al., *Emulsion Synthesis of Size-Tunable CH3NH3PbBr3 Quantum Dots: An Alternative Route toward Efficient Light-Emitting Diodes.* ACS Applied Materials & Interfaces, 2015. **7**(51): p. 28128-28133.

33. Hoshi, K., et al., *Purification of Perovskite Quantum Dots Using Low-Dielectric-Constant Washing Solvent "Diglyme" for Highly Efficient Light-Emitting Devices.* ACS Applied Materials & Interfaces, 2018. **10**(29): p. 24607-24612.

34. Li, J., et al., *50-Fold EQE Improvement up to 6.27% of Solution-Processed All-Inorganic Perovskite CsPbBr3 QLEDs via Surface Ligand Density Control.* 2017. **29**(5): p. 1603885.

35. Swarnkar, A., et al., *Quantum dot–induced phase stabilization of α-CsPbI$_3$ perovskite for high-efficiency photovoltaics.* 2016. **354**(6308): p. 92-95.

36. Zhao, Q., et al., *High efficiency perovskite quantum dot solar cells with charge separating heterostructure.* Nature Communications, 2019. **10**(1): p. 2842.

37. Yilbas, B.S., A. Al-Sharafi, and H. Ali, *Chapter 3 - Surfaces for Self-Cleaning*, in *Self-Cleaning of Surfaces and Water Droplet Mobility*, B.S. Yilbas, A. Al-Sharafi, and H. Ali, Editors. 2019, Elsevier. p. 45-98.

38. Wang, X.-j., et al., *Construction of amorphous TiO2/BiOBr heterojunctions via facets coupling for enhanced photocatalytic activity.* Journal of Hazardous Materials, 2015. **292**: p. 126-136.

39. Zhou, L., et al., *Insight into the effect of ligand-exchange on colloidal CsPbBr3 perovskite quantum dot/mesoporous-TiO2 composite-based photodetectors: much faster electron injection.* Journal of Materials Chemistry C, 2017. **5**(25): p. 6224-6233.

40. Lee, S., et al., *Thin Amorphous TiO2 Shell on CdSe Nanocrystal Quantum Dots Enhances Photocatalysis of Hydrogen Evolution from Water.* The Journal of Physical Chemistry C, 2014. **118**(41): p. 23627-23634.

41. Dibenedetto, C.N., et al., *PbS Quantum Dots Decorating TiO(2) Nanocrystals: Synthesis, Topology, and Optical Properties of the Colloidal Hybrid Architecture.* Molecules, 2020. **25**(12).

42. Wei, Y., Z. Cheng, and J. Lin, *An overview on enhancing the stability of lead halide perovskite quantum dots and their applications in phosphor-converted LEDs.* Chemical Society Reviews, 2019. **48**(1): p. 310-350.

VITA

NAME	Chutikan Sairot
DATE OF BIRTH	07/06/2539
PLACE OF BIRTH	Tak
INSTITUTIONS ATTENDED	Chulalongkorn university
HOME ADDRESS	1198/230, The Base Sukhumvit 50, 2 Khwaeng Phra Khanong, Khet Khlong Toei, Krung Thep Maha Nakhon 123, Bangkok Noi, Bangkok - 10260, Thailand.

จุฬาลงกรณ์มหาวิทยาลัย

CHULALONGKORN UNIVERSITY